

Article

Parametric Investigation of Particle Swarm Optimization to Improve the Performance of the Adaptive Neuro-Fuzzy Inference System in Determining the Buckling Capacity of Circular Opening Steel Beams

Quang Hung Nguyen ^{1,*}, Hai-Bang Ly ^{2,*}, Tien-Thinh Le ^{3,*}, Thuy-Anh Nguyen ², Viet-Hung Phan ⁴, Van Quan Tran ² and Binh Thai Pham ²

¹ Thuyloi University, Hanoi 100000, Vietnam

² University of Transport Technology, Hanoi 100000, Vietnam; anhnt@utt.edu.vn (T.-A.N.); quantv@utt.edu.vn (V.Q.T.); binhpt@utt.edu.vn (B.T.P.)

³ Institute of Research and Development, Duy Tan University, Da Nang 550000, Vietnam

⁴ University of Transport and Communications, Ha Noi 100000, Vietnam; phanviethung@utc.edu.vn

* Correspondence: hungwuhan@tlu.edu.vn (Q.H.N.); banglh@utt.edu.vn (H.-B.L.); letienthinh@duytan.edu.vn (T.-T.L.)

Received: 20 April 2020; Accepted: 6 May 2020; Published: 12 May 2020



Abstract: In this paper, the main objectives are to investigate and select the most suitable parameters used in particle swarm optimization (PSO), namely the number of rules (n_{rule}), population size (n_{pop}), initial weight (w_{ini}), personal learning coefficient (c_1), global learning coefficient (c_2), and velocity limits (f_v), in order to improve the performance of the adaptive neuro-fuzzy inference system in determining the buckling capacity of circular opening steel beams. This is an important mechanical property in terms of the safety of structures under subjected loads. An available database of 3645 data samples was used for generation of training (70%) and testing (30%) datasets. Monte Carlo simulations, which are natural variability generators, were used in the training phase of the algorithm. Various statistical measurements, such as root mean square error (RMSE), mean absolute error (MAE), Willmott's index of agreement (IA), and Pearson's coefficient of correlation (R), were used to evaluate the performance of the models. The results of the study show that the performance of ANFIS optimized by PSO (ANFIS-PSO) is suitable for determining the buckling capacity of circular opening steel beams, but is very sensitive under different PSO investigation and selection parameters. The findings of this study show that $n_{rule} = 10$, $n_{pop} = 50$, $w_{ini} = 0.1$ to 0.4 , $c_1 = [1, 1.4]$, $c_2 = [1.8, 2]$, $f_v = 0.1$, which are the most suitable selection values to ensure the best performance for ANFIS-PSO. In short, this study might help in selection of suitable PSO parameters for optimization of the ANFIS model.

Keywords: particle swarm parameters; adaptive neuro-fuzzy inference system; circular opening steel beams; buckling capacity

1. Introduction

Circular opening steel beams have been increasingly acknowledged in structural engineering because of their many remarkable advantages [1], including their ability to bridge the span of a large aperture or their lighter weight compared with conventional steel beams. In general, the industrial approach to producing such a structural member is the rolled method, involving a single steel piece. This is then cut so that the two halves can be assembled, making an I-section, which is also called an H-section steel beam. Hoffman et al. [2] showed that the flexural stiffness and specific gravity per unit

length was improved significantly in circular opening steel beams structures. In addition, economic and aesthetics factors are also beneficial points that deserve significant attention [3,4]. A typical structural member has a regular circular openings along its length [1–8], and is about 40–60% deeper and 40–60% stronger than a regular I-section [5,6]. Because of these advantages, circular beams are not only used in lightweight or large-span structures, but are also used for other complex civil engineering structures, such as bridges [9]. Due to the possibility of using circular opening steel beams in various engineering applications, investigation of the failure behavior is crucial to ensure the safety of structures. Several previously published studies on the failure modes of circular beams, for instance the work by Sonck et al. [3], have shown that the web openings are the leading causes of the complex failure behavior of cellular beams, including web post-buckling (WPB), the Vierendeel mechanism (VM), rupture of the web post-weld [1], local web buckling (LWB), and web distortional buckling (WDB) [5,6].

Miscellaneous analysis-related research studies have been conducted to study the behavior of circular opening steel beams [10–12], which have mainly focused on the web openings using various numerical approaches [7,9]. As an example, Chung et al. [11] used finite element models with material and geometrical nonlinearity to calculate the behavior of circular beams, resulting in approximately 15.8% of error. Numerical methods help create various case studies in order to gain more knowledge about the working principles of the structures. Taking the work of Panedpojaman and Thepchatrri [4] as an example, the authors created a total of 408 nonlinear finite element models using ANSYS software to investigate the behavior of circular steel beams. The results indicated that there is always a small difference between the finite element model and the theoretical formulation. In another study, Sonck et al. [3] generated 597 numerical models, which were calibrated with laboratory tests for 14 geometrically different full-scale steel cellular beams and verified with 1948 numerical analyzes. The results showed that the experimental and numerical curves were identical, with a maximum load gap range of 5.1% to 6.5%. Typically, the numerical models are useful for evaluating the behavior of circular beams [1,3,6,9,13]. However, these model require much effort and the use of modern software and equipment.

Machine learning (ML) algorithms, a branch of artificial intelligence (AI) techniques, have been constantly developed during the past few decades due to the significant increase in computer science [14–21]. Various ML models have been effectively implemented to solve countless specific engineering problems, including in material sciences [22–24], geotechnical engineering [25–29], and especially structural engineering [18,30–32]. As an example, Vahid et al. [33] selected an artificial neural network (ANN) algorithm, the most popular ML model, to predict the shear capacity of a web opening steel I-beam. The proposed ANN model had better accuracy compared with other existing formulas or theoretical predictions derived from the ACI 318-08 standard. Abambres et al. [34] also used the ANN method to investigate the buckling load capacity of cellular beams under uniformly distributed vertical loads, using eight geometrical parameters. Good results were achieved by the ANN, giving 3.7% for the total error and 0.4% for the average relative error. Blachowski and Pnevmatikos [35] proposed an ANN model for the design and control of the vibration of structural elements under earthquake loading. In the same context of seismic excitation, Pnevmatikos and Thomos [36] employed a stochastic control approach to determine the influence of random characters on the dynamic behavior of engineering structures. The neuro-fuzzy system is another efficient ML algorithm, which has been employed in many structural and material engineering applications, including for steel structures. Seitllari and Naser [37] investigated the performance of an adaptive neuro-fuzzy inference system (ANFIS) in predicting a fire-induced spalling phenomenon in steel-reinforced concrete structures. Naser [38] derived a material model for steel structures, taking into account the dependency of temperature based on machine learning techniques. Basarir et al. [39] compared the performance between conventional regression techniques and ANFIS in predicting the ultimate pure bending of concrete-filled steel tubular members. Naderpour and Mirrashid [40] used ANFIS to predict the shear strength of beams that had been reinforced with steel stirrups. Mermerdaş et al. [41] applied ANFIS

to evaluate the flexural behavior of steel circular hollow section (CHS) beams. It was stated that the ANFIS was a promising tool for quick and accurate evaluation of the mechanical behavior of steel-based engineering structures.

In general, the ML algorithms are excellent and effective for evaluating the behavior of structural members, including circular beams. However, their performance depends significantly on the selection of parameters used to learn the models [42]. Therefore, the process of determining such parameters is crucial to obtain highly reliable and accurate prediction results. Concerning the ANN, many parameters could be involved, such as the initial weights, biases to start the training phase, the learning rate, the stopping criterion, the choice of features in the training phase, the choice of the splitting dataset ratio, the number of hidden layers and the corresponding activation functions, the training algorithm, and the number of neurons in each hidden layer [43–45]. Considering the ANFIS, two groups of parameters can be considered, namely the nonlinear parameters of the antecedent membership function (MF) and linear parameters of the consequent MF, which depends on the partitioning of the fuzzy space, as well as the type of Sugeno model [46,47]. Besides, many optimization techniques, such as particle swarm optimization (PSO), differential evolution (DE), evolutionary algorithm (EA), genetic algorithm (GA), artificial bee colony (ABC) or cuckoo search (CS) techniques, have been proposed to optimize the parameters of the ML models [48,49]. Each optimization technique also possesses many different parameters that need to be tuned to obtain good prediction performances, including the time required to adjust the combination of these parameters [48,49]. Among the well-known optimization techniques, PSO is considered as one of the most popular and effective techniques [50]. Many hybrid ML algorithms have used PSO for the parameter tuning process, including ANN, ANFIS, and Support Vector Machine (SVM) algorithms [51–53]. In the literature, limited studies have used ANFIS optimized by PSO (ANFIS-PSO) to predict the mechanical properties of structural members. Moreover, a systematic investigation of ANFIS-PSO parameters under random sampling has not been performed, as the sampling method has been proven to greatly affect the accuracy of the ML algorithms [54].

In this study, the main purpose was to carry out a parametric investigation of PSO parameters to improve the performance of ANFIS in predicting the buckling capacity of circular opening steel beams, which is an important mechanical property that is crucial for the safety of structures under subjected loads. The database used in this work consisted of 3645 data samples, which were derived from numerical results using ANSYS and available in the literature. The parametric studies were carried out with the help of Monte Carlo simulations, which are natural variability generators, in the training phase of the algorithm. Various statistical measurements, such as the root mean square error (RMSE), mean absolute error (MAE), Willmott's index of agreement (IA), and Pearson's coefficient of correlation (R), were used to evaluate the performance of the model.

2. Novelty and Significance of This Study

As reported in the introduction, the estimation of the buckling capacity of circular opening steel beams is important for the safety of structures under subjected loads. As instability is a complex (nonlinear) problem that is affected by various parameters, the determination of the critical buckling load remains challenge for researchers (engineers) in the fields of mechanics and civil engineering. Despite various experimental works having investigated this problem, it is not easy to derive a generalized expression that considers all the parameters that govern the instability of circular opening steel beams. To overcome this difficulty, the use of ML techniques, such as ANFIS optimized by the PSO algorithm proposed in this study, could be a good choice as a surrogate model. This soft computing method could help to explore the nonlinear relationships between the buckling capacity and the input variables, especially the geometrical parameters of the beams. In addition, the investigation of PSO parameters based on the Monte Carlo random sampling technique could contribute to better knowledge on selection of suitable parameters to achieve better performance with the PSO algorithm, which could be further recommended for other problems. Finally, the proposed ML-based model

could be a potential tool for researchers or structural engineers in accurately estimating the buckling capacity of circular opening steel beams, which could (i) work within the ranges of values used in this study for the input variables and (ii) save time and costs in development of other numerical schemes (i.e., finite element models).

3. Database Construction

The database in this study was obtained by analyzing 3645 different configurations of circular opening steel beams (Figure 1). It should be noted that the database was extracted from a validated finite element model, which was previously proposed in the literature by Abambres et al. [34]. It consisted of 8 input parameters, namely the length of the beam (denoted as L), the end opening distance (denoted as d_0), circular opening diameter (denoted as D), the inter-opening distance (denoted as d), the height of the section (denoted as H), the thickness of the web (denoted as t_{web}), the width of the flange (denoted as w_{flange}), the thickness of the flange (denoted as t_{flange}), and the buckling capacity, which was considered as the target variable (denoted as P_u). It should be pointed out that the database was generated for one material type (with a typical Young's modulus of 210 GPa and Poisson's ratio of 0.3). The results of the statistical analysis of the P_u and the corresponding influential parameters are presented in Table 1.

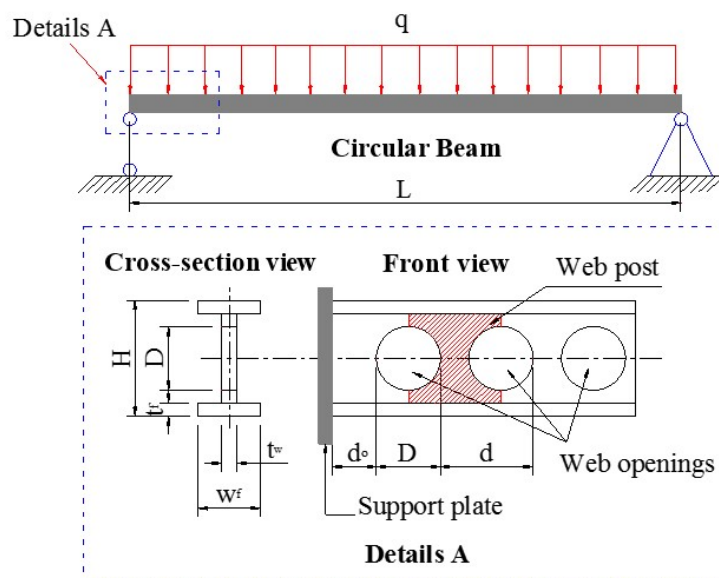


Figure 1. Diagram of circular opening steel beam under uniform loading and its geometrical parameters.

Table 1. Initial statistical analysis of the dataset.

Variable	Length of Beam	End Opening Distance	Opening Diameter	Inter-Opening Distance	Height of Section	Thickness of Web	Width of Flange	Thickness of Flange	Buckling Capacity
Symbol	L	d_0	D	d	H	t_{web}	w_{flange}	t_{flange}	P_u
Unit	m	mm	mm	mm	mm	mm	mm	mm	N/m
Role	Input	Input	Input	Input	Input	Input	Input	Input	Output
Min	4.0	12.0	247.0	24.70	420.00	9.0	162.0	15.0	26.4
MD ^a	6.0	256.5	373.0	108.17	560.00	12.0	216.0	20.0	169.3
Max	8.0	718.0	560.0	274.40	700.00	15.0	270.0	25.0	1361.7
Mean	6.0	265.4	383.6	112.51	560.00	12.0	216.0	20.0	225.7
SD ^b	1.4	157.5	93.0	68.51	114.33	2.5	44.1	4.1	182.5
CV ^c	23.6	59.3	24.2	60.90	20.42	20.4	20.4	20.4	80.9

^a Median. ^b Standard deviation. ^c Coefficient of variation (%).

The input and target variables in this work were scaled in the range of [0, 1] to minimize the numerical bias of the dataset. After performing the simulation part, a transformation into the normal range was conducted to better interpret the obtained results. Concerning the development phase, the dataset was split into two parts, namely the training part (70% of the total data) and the testing part (the remaining 30% of the data), which served as the learning and validation phases of the proposed ANFIS-PSO model, respectively.

4. Machine Learning Methods

4.1. Adaptive Neuro-Fuzzy Inference System

Jang et al. [55] introduced the fuzzy adaptive system of adaptive neurology, called ANFIS, as an improved ML method and a data-driven modeling approach to evaluate the behavior of complex dynamic systems [56,57]. ANFIS aims to systematically generate unknown fuzzy rules from a given set of input and output data. ANFIS creates a functional map that approximates the internal system parameter estimation method [58–60]. Fuzzy systems are rule-based systems developed from a set of language rules. These systems can represent any system with good accuracy and are, therefore, considered to be universal approximators. Thus, ANFIS is the most popular neuro-fuzzy hybrid network used for the modeling of complex systems. The ANFIS model's main strength is that it is a universal approximator with the ability to request interpretable "if-then" rules [61]. In ANFIS, a Sugeno-type fuzzy system was used to construct the five-layer network.

4.2. Particle Swarm Optimization (PSO)

Eberhart and Kennedy developed the PSO algorithm in 1995. It is an evolutionary computing technique with a particular enhancement method, population collaboration, and competition based on the simulation of simplified social models, such as bird flocking, fish schooling, and swarming theory [62–65]. It is a biological-based algorithm that shapes bird flocking social dynamics large number of birds flock synchronously, suddenly change direction, iteratively scatter and group, and eventually perch on a target. The PSO algorithm supports simple rules for bird flocking and acts as an optimizer for nonlinear continuous functions [66]. PSO has gained much attention and has been successfully applied in various fields, especially for unconstrained continuous optimization problems [67]. Indeed, in PSO, a swarm member, also called a particle, is a potential solution, which is used as a search space point. The global equilibrium is known as the food position. The particle has a fitness value and a speed with which to change its flight path for the best swarm experiences to find the global optimum in the D-dimensional solution space. The PSO algorithm is easy to implement and many optimization problems have been empirically shown to perform well [68]. However, its performance depends significantly on the algorithm parameters described below.

4.2.1. Initial Weight (w_{ini})

The particle in the PSO is represented as a real-valued vector containing an instance of all parameters that characterize the problem of optimization. By flying a number of particles, called a swarm, the PSO explores the solution space. The initial swarm is generated at random, and generally consecutive iterations maintain a consistent swarm size. The swarm of particles looks for the optimum target solution in each iteration by referring to past experiences.

4.2.2. Cognition Learning Rate (Personal Learning Coefficient— c_1)

PSO enriches swarm intelligence by storing the best positions that each particle has visited so far. Particles recall the best position among those it met, called p_{best} , and the best positions of its neighbors. There are two variants, namely l_{best} and g_{best} , used to hold the neighbors in the best position. The particle in the local version keeps track of the best l_{best} location obtained by its neighboring local

particles. For the global version, any particles in the whole swarm will determine the best location for gbest. Therefore, the gbest model is the lbest model's special case.

4.2.3. Social Learning Rate (Global Learning Coefficient— c_2)

PSO starts with the random initialization in the search space of a population (swarm) of individuals (particles) and operates on the particles' social behavior in the swarm. Consequently, it finds the best global solution by simply adjusting each individual's trajectory to their own best location and to the best swarm particle in each phase (generation). Nevertheless, the trajectory of each particle in the search space is modified according to their own flying experience and the flying experience of the other particles in the search space by dynamically altering the velocity of each particle.

4.2.4. Number of Particles (Population Size— n_{pop})

The location and speed of the i th particle can be expressed in the dimensional search space. Every particle has its own best (pbest) location, according to the best personal objective value at the time t . The world's best particle (gbest) is the best particle found at time t in the entire swarm.

4.2.5. Velocity Limits (f_v)

Each particle's new speed is determined as follows:

$$y_{ij}(t+1) = wy_{ij}(t) + c_1r_1(p_{ij} - x_{ij}(t)) + c_2r_2(p_{gj} - x_{ij}(t)); \quad j = 1, 2, \dots, d \quad (1)$$

where c_1 and c_2 are constants referred to as acceleration coefficients, w is referred to as the inertia factor, and r_1 and r_2 are two independent random numbers distributed evenly within the spectrum. The location of each particle is, thus, modified according to the following equation in each generation:

$$a_{ij}(t+1) = a_{ij}(t) + y_{ij}(t+1), \quad j = 1, 2, 3, \dots, d \quad (2)$$

In the standard PSO, Equation (1) is used to calculate the new velocity according to its previous velocity and to the distance of its current position from both its own best historical position and its neighbors' best positions. The value of each factor in Y_i can be clamped within the range to monitor excessive particles roaming outside the search area, then the particle flies toward a new location.

4.3. Monte Carlo Simulation

The Monte Carlo technique has been commonly used as a variability generator in the training phase of the algorithm, taking into account the randomness of the input space [69–72]. Hun et al. [73] studied the problem of crack propagation in heterogeneous media within a probabilistic context using Monte Carlo simulations. Additionally, Capillon et al. [74] investigated an uncertainty problem in structural dynamics for composite structures using Monte Carlo simulations. Overall, the Monte Carlo method has been successfully applied to take into account the randomness in the field of mechanics [75–80]. The key point of the Monte Carlo method is to repeat the simulations many times to calculate the output responses by randomly choosing values of the input variables in the corresponding space [81,82]. In this manner, all information about the fluctuations in the input space can be transferred to the output response. In this work, a massive numerical parallelization scheme was programmed to conduct the randomness propagation process. The statistical convergence of the Monte Carlo method reflects whether the number of simulations is sufficient, which can be defined as follows [83–85]:

$$f_{conv} = \frac{100}{m\underline{S}} \sum_{j=1}^m S_j \quad (3)$$

where m is the number of Monte Carlo iterations, S is the random variable considered, and \underline{S} is the average value of S .

4.4. Quality Assessment Criteria

In the present work, three quality assessment criteria—the correlation coefficient (R), root mean squared error (RMSE), and mean absolute error (MAE)—have been used in order to validate and test the developed AI models. R^2 allows us to identify the statistical relationship between two data points and can be calculated using the following equation [86–92]:

$$R = \frac{\sum_{j=1}^N (y_{0,j} - \bar{y})(y_{p,j} - \bar{y})}{\sqrt{\sum_{j=1}^N (y_{0,j} - \bar{y})^2 \sum_{j=1}^N (y_{p,j} - \bar{y})^2}} \quad (4)$$

where N is the number of observations, y_p and \bar{y} are the predicted and mean predicted values, while y_0 and \bar{y} are the measured and mean measured values of Young's modulus of the nanocomposite, respective $j = 1:N$. In the case of RMSE and MAE, which have the same units as the values being estimated, low value for RMSE and MAE basically indicate good accuracy of the models' prediction output [93,94]. In an ideal prediction, RMSE and MAE should be zero. RMSE and MAE are given by the following formulae [95–99]:

$$\text{RMSE} = \sqrt{\sum_{i=1}^N (y_0 - y_p)^2 / N} \quad (5)$$

$$\text{MAE} = \frac{1}{N} \sum_{i=1}^N |y_0 - y_p| \quad (6)$$

In addition, the Willmott's index of agreement (IA) has also been employed in this study. The formulation of IA is given by [100,101]:

$$\text{IA} = 1 - \frac{\sum_{i=1}^N (y_0 - y_p)^2}{\sum_{i=1}^N (|y_0 - \bar{y}| + |y_p - \bar{y}|)^2} \quad (7)$$

5. Results and Discussion

5.1. Description of Parametric Studies

In order to investigate the influence of PSO parameters on the performance of ANFIS, parametric studies were carried out by varying n_{rule} , n_{pop} , w_{ini} , c_1 , c_2 , and f_v , as indicated in Table 2. It is noteworthy that the proposed range was selected by considering both problem dimensionality (i.e., complexity) and computation time. As recommended by He et al. [102] and Chen et al. [48], the PSO initial weight should be carefully investigated. Therefore, a broad range of w_{ini} was proposed, ranging from 0.1 to 1.2. The number of populations varied from 20 to 300 with a nonconstant step, whereas the coefficients c_1 and c_2 ranged from 0.2 to 2 with a resolution of 0.2. The number of fuzzy rules varied from 5 to 40. Finally, the f_v ranged from 0.05 to 0.2.

The relationship between the number of fuzzy rules and the number of total ANFIS weight parameters is depicted in Figure 2. As can be seen, the relationship is linear, showing that as the number of fuzzy rules increases, the number of ANFIS weight parameters increases. For illustration purposes, the number of weight parameters increases from 50 to 370, while the number of fuzzy rules increases from 5 to 40. Additionally, the characteristics of the ANFIS structure are described in Table 3, showing that the Gaussian membership function was used to generate fuzzy rules.

Table 2. Values used for parameters in parametric studies.

Parameters	Values Used											
n_{rule}	5	10	15	20	30	40						
n_{pop}	20	40	60	80	100	150	200	250	300			
w_{ini}	0.1	0.2	0.3	0.4	0.5	0.6	0.7	0.8	0.9	1	1.1	1.2
c_1	0.2	0.4	0.6	0.8	1	1.2	1.4	1.6	1.8	2		
c_2	0.2	0.4	0.6	0.8	1	1.2	1.4	1.6	1.8	2		
f_v	0.05	0.1	0.15	0.2								

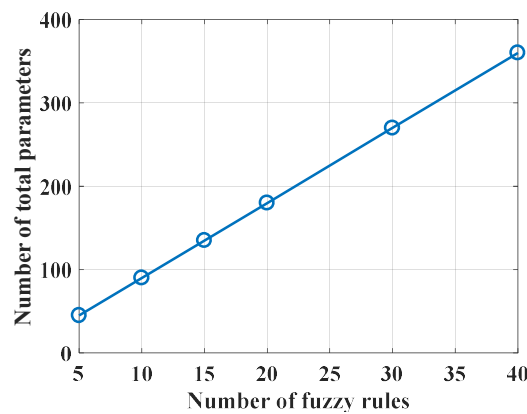


Figure 2. Influence of the number of fuzzy rules on the number of total ANFIS weight parameters to be optimized by PSO.

Table 3. Characteristics of ANFIS structure.

Parameter	Description
Number of inputs	8
Number of outputs	1
Input membership function type	Gaussian
Number of parameter per membership function	2
Number of fuzzy rules	n_{rule}
Output membership function type	Linear
Number of nonlinear parameters	$8 \times 2 \times n_{rule}$
Number of linear parameters	$9 \times n_{rule}$
Number of total parameters	$25 \times n_{rule}$

5.2. Preliminary Analyses

5.2.1. Computation Time

Figure 3 presents the influence of n_{rule} and swarm parameters on the computation time. It is worth noting that the running time was scaled with respect to the minimum value of the corresponding parameter. For instance, the computation time using $n_{rule} = 10$ is two times larger than the case using $n_{rule} = 5$. Additionally, in Figure 3, it is seen that n_{rule} and n_{pop} exhibited the highest slope (about 0.75), confirming that these two parameters required considerable computation time. For all other parameters, the computation time remained constant when increasing the value of the parameter.

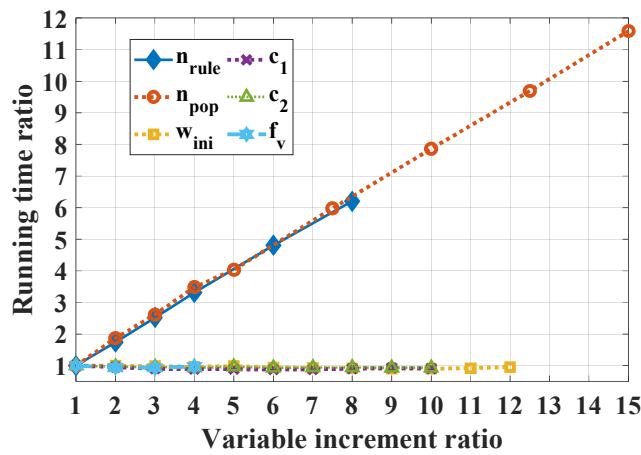


Figure 3. Influence of variable increment ratio on running time, noting that both n_{rule} and n_{pop} exhibit a slope coefficient of 0.75.

5.2.2. PSO Stopping Criterion

In this study, 1000 iterations were applied as a stopping criterion in the optimization problem for the weight parameters of ANFIS. Figure 4 shows the convergence of statistical criteria in the function of n_{rule} , whereas Figure 5 presents the convergence of these criteria regarding n_{pop} . For the evaluation of RMSE, MAE, and R over 1000 iterations in 6 cases for different n_{rule} , the training parts are given in Figure 4a–c, whereas the testing parts are displayed in Figure 4d–f. It was observed that at least 800 iterations were required to obtain convergence results for RMSE, MAE, and R for all the cases. However, no specific trend could be deduced in order to obtain the best n_{rule} parameter. Finally, it is worth noting that for all the cases of n_{rule} , the values of RMSE, MAE, and R for the testing part were very close. Indeed, the values of RMSE for the testing part ranged from 0.038 to 0.043, the values of MAE for the testing part varied from 0.015 to 0.022, and those of R ranged from 0.95 to 0.97. The evaluation of RMSE, MAE, R over 1000 iterations in 9 cases of n_{pop} is shown (Figure 5). Similar results were obtained as for n_{rule} . At least 800 iterations were needed to obtain the convergence results.

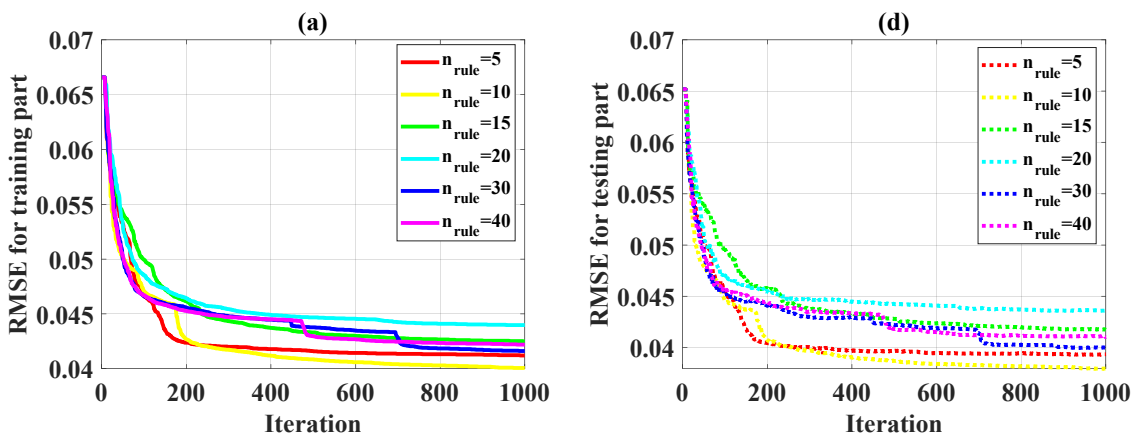


Figure 4. Cont.

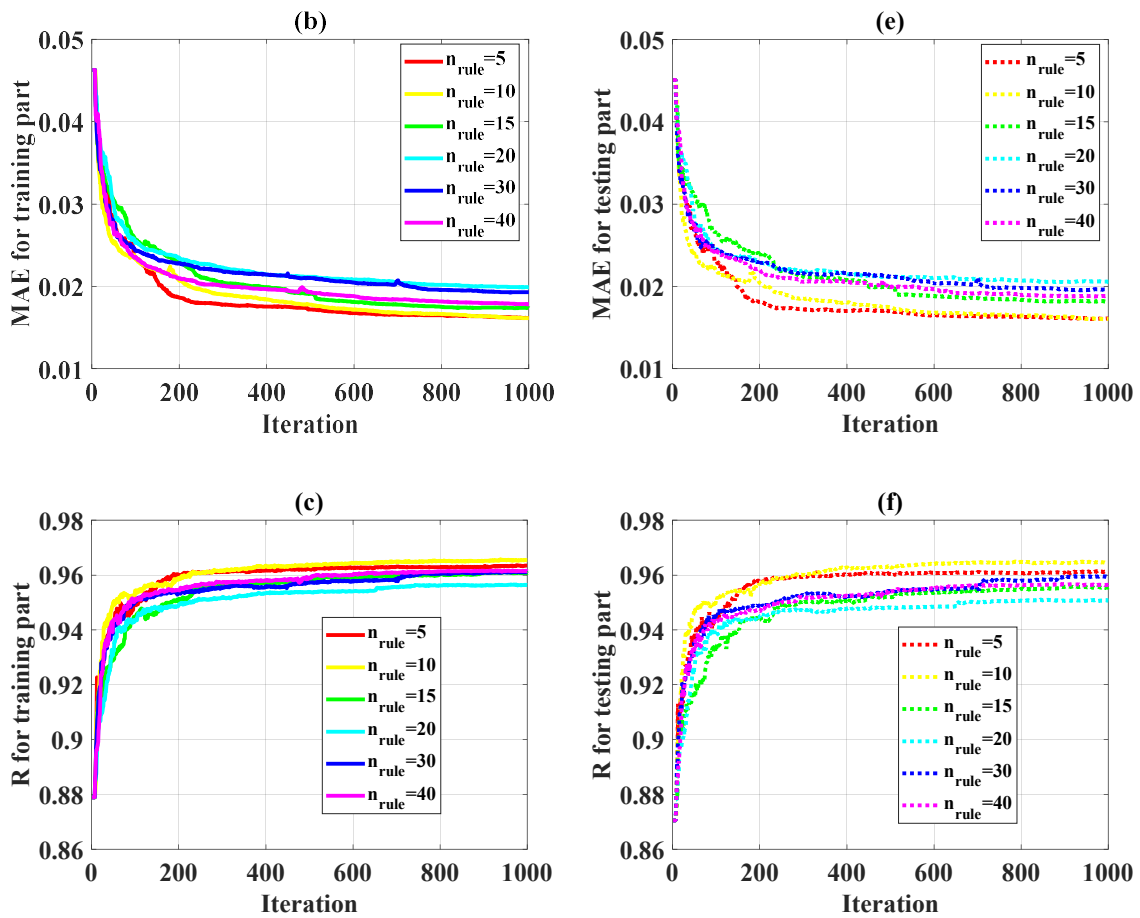


Figure 4. Convergence of several statistical criteria over 1000 iterations in terms of n_{rule} for the training part: (a) RMSE, (b) MAE, (c) R. Convergence of several statistical criteria over 1000 iterations in terms of n_{rule} for the testing part: (d) RMSE, (e) MAE, (f) R.

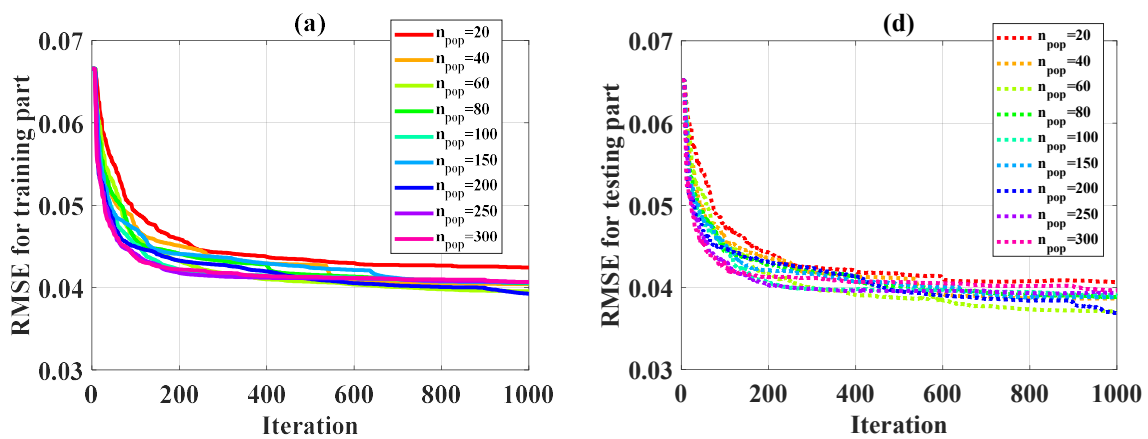


Figure 5. Cont.

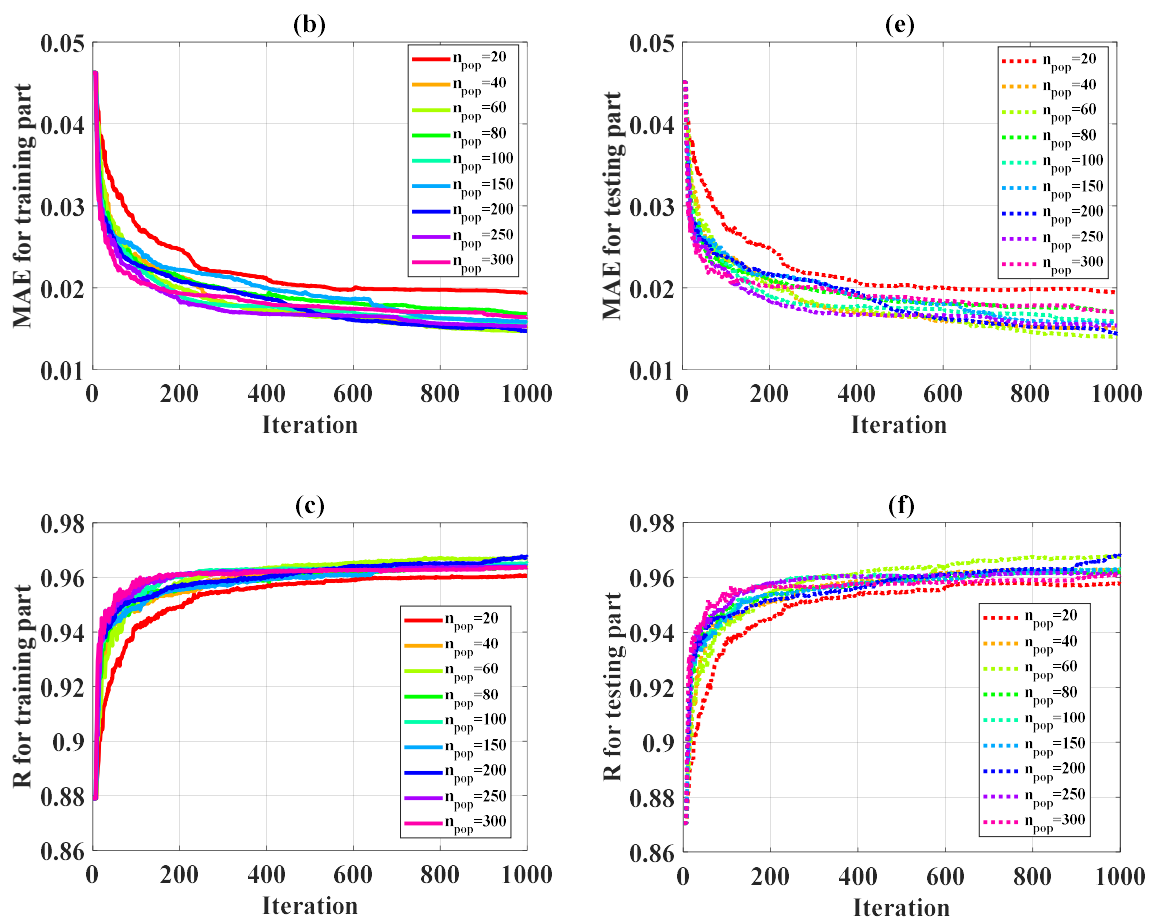


Figure 5. Convergence of several statistical criteria over 1000 iterations in terms of n_{pop} for the training part: (a) RMSE, (b) MAE, (c) R. Convergence of several statistical criteria over 1000 iterations in terms of n_{pop} for the testing part: (d) RMSE, (e) MAE, (f) R.

5.2.3. Statistical Convergence

In order to take into account variability in the input space, 200 random realizations were performed for each configuration. These realizations increased the influence of the probability density function of inputs on the optimization results. In terms of n_{rule} , Figure 6a–c indicate the statistical convergence of RMSE, MAE, and R for the training part, whereas Figure 6d–f present the statistical convergence of the same parameters for the testing part, respectively. It can be seen that after about 100 random realizations, statistical convergence was reached, which was correct for all the tested cases. Similarly, Figure 7 shows the statistical convergence in terms of n_{pop} for both training and testing parts. Similarly, 200 random realizations were observed to be sufficient to achieve reliable results.

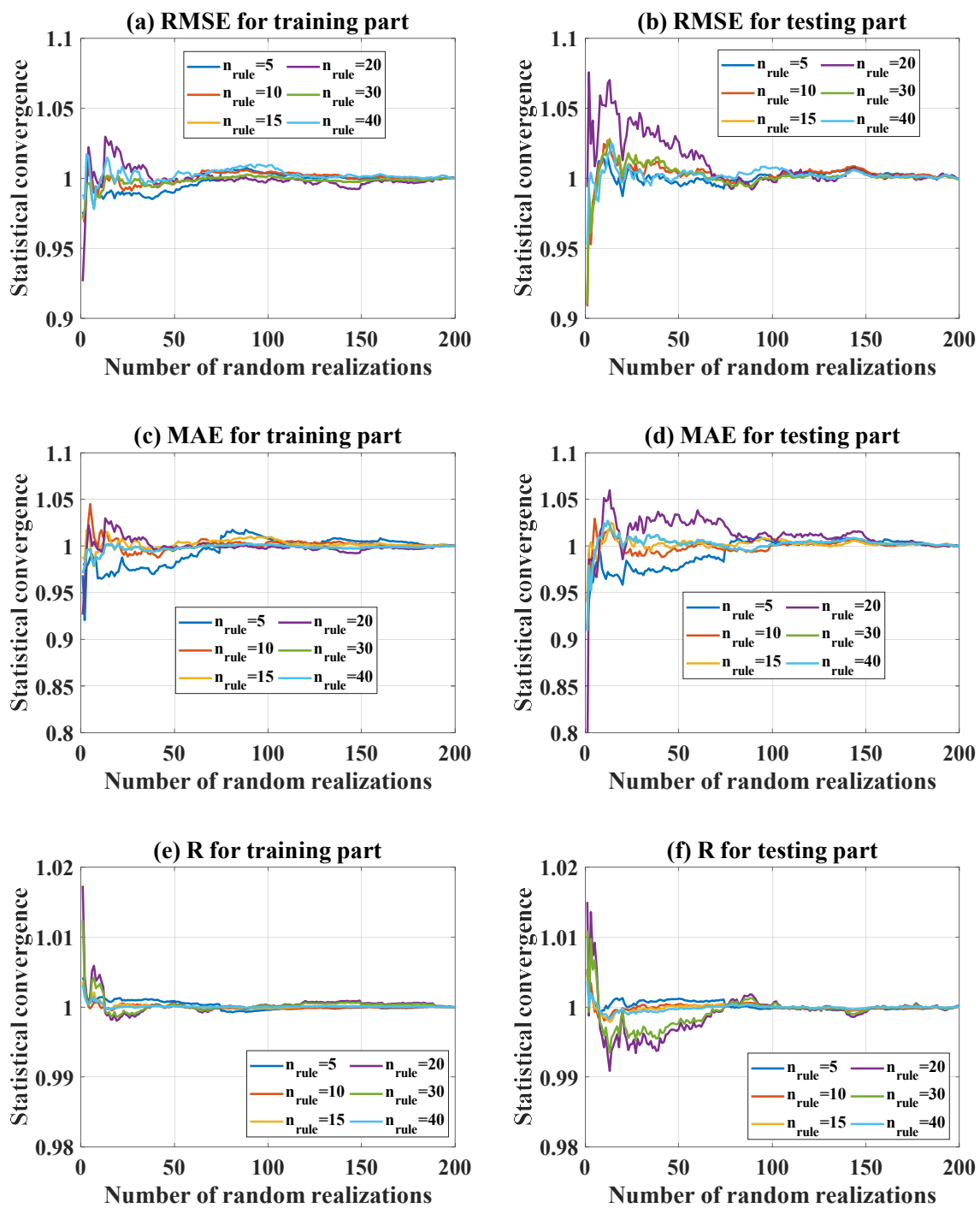


Figure 6. Statistical convergence over 200 random realizations in terms of n_{rule} for the training part: (a) RMSE, (b) MAE, (c) R. Statistical convergence over 200 random realizations in terms of n_{rule} for the testing part: (d) RMSE, (e) MAE, (f) R.

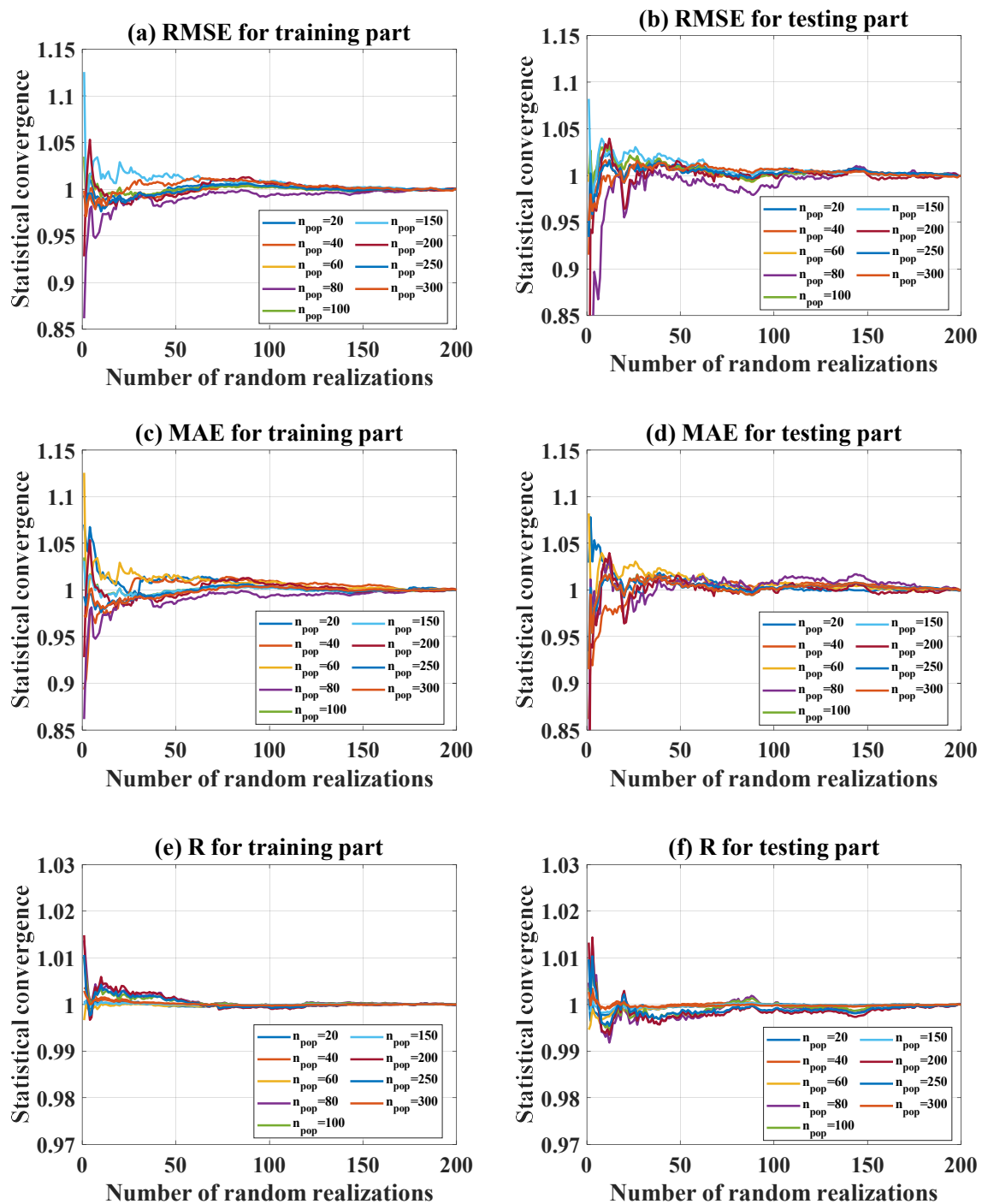


Figure 7. Statistical convergence over 200 random realizations in terms of n_{pop} for the training part: (a) RMSE, (b) MAE, (c) R. Statistical convergence over 200 random realizations in terms of n_{pop} for the testing part: (d) RMSE, (e) MAE, (f) R.

5.3. Parametric Performance

5.3.1. Influence of Number of Rules (n_{rule})

The evaluation of RMSE, MAE, R, and IA in the function of n_{rule} is presented in Figure 8a–d, respectively, for both training and testing parts. It can be seen that the accuracy of the ANFIS-PSO reduced when the number of n_{rule} increased (i.e., RMSE and MAE increased, while R and IA decreased). It is worth noting that the higher the number of rules, the larger dimensionality of the problem

(Figure 2). Therefore, regarding the total number of ANFIS weight parameters, the computation time, and the average value of the statistical criteria (RMSE, MAE, R, and IA), $n_{\text{rule}} = 10$ was considered as the most appropriate value.

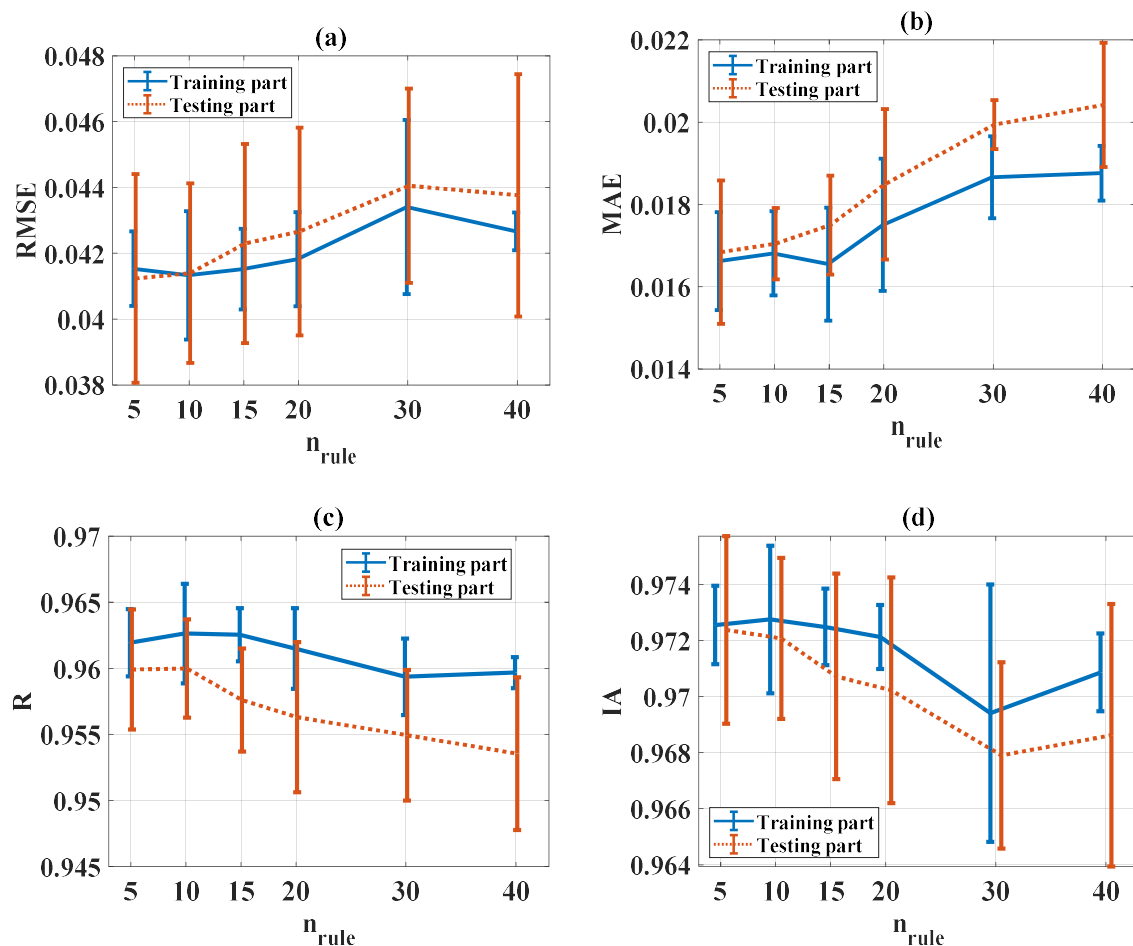


Figure 8. Evaluation of statistical criteria in the function of n_{rule} : (a) RMSE, (b) MAE, (c) R, and (d) IA.

5.3.2. Influence of Population Number (n_{pop})

The evaluation of statistical criteria in the function of n_{pop} for RMSE, MAE, R, and IA is shown in Figure 9a–d, respectively, for both training and testing parts. It can be seen that except for the low value for population size (i.e., $n_{\text{pop}} = 20$), all other n_{pop} values show good prediction results, especially for $n_{\text{pop}} = 200$. However, as introduced in the preliminary analyses for computation time, the higher the number of n_{pop} , the more time is consumed. Finally, $n_{\text{pop}} = 50$ was chosen as the most appropriate average value for statistical criteria and computation time.

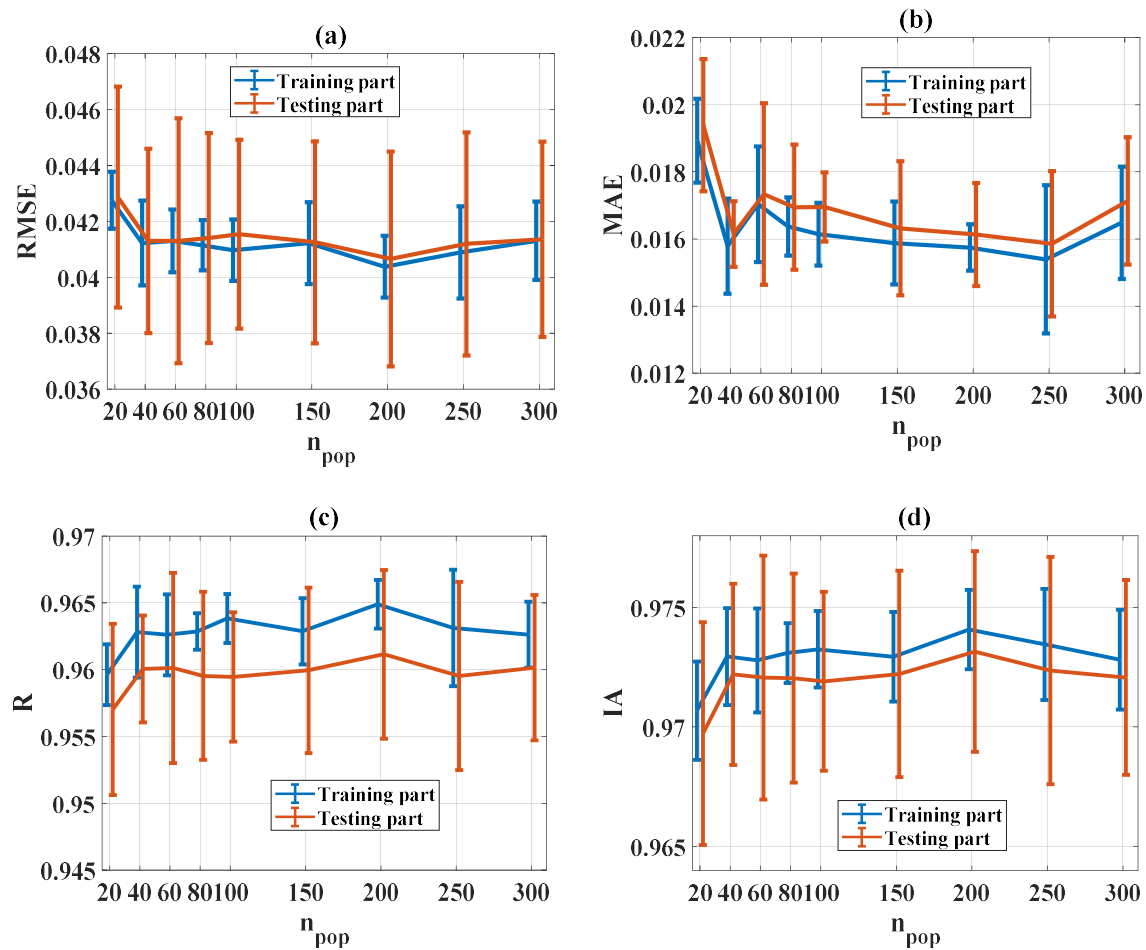


Figure 9. Evaluation of statistical criteria in the function of n_{pop} : (a) RMSE, (b) MAE, (c) R, and (d) IA.

5.3.3. Influence of Initial Weight (w_{ini})

The evaluation of statistical criteria in the function of w_{ini} for RMSE, MAE, R, and IA is shown in Figure 10a–d, respectively, for both training and testing parts. It can be seen that poor prediction performance was obtained when w_{ini} was larger than 0.5 (i.e., an increase of RMSE and MAE values and a decrease of R and IA values). Regarding the statistical criteria (RMSE, MAE, R, and IA), a w_{ini} value range of between 0.1 and 0.4 was the most appropriate.

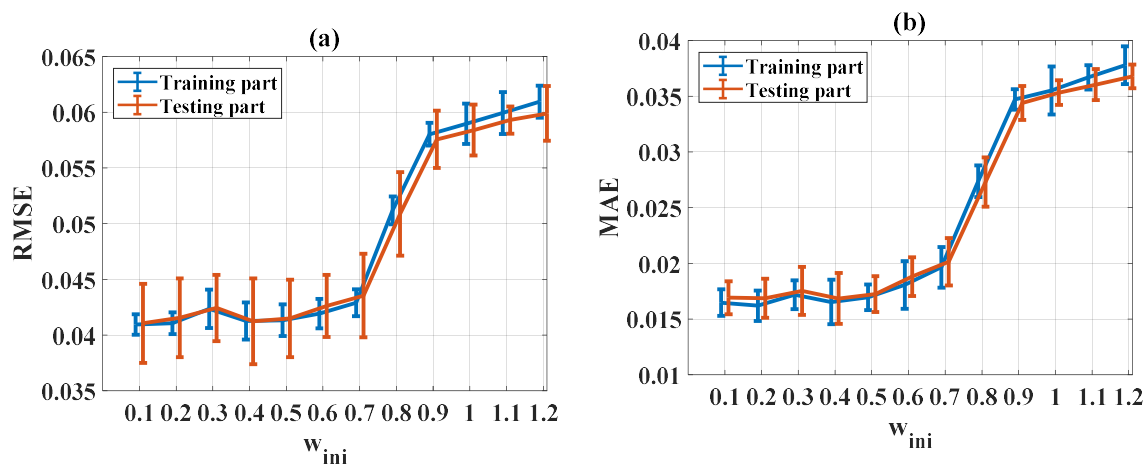


Figure 10. Cont.

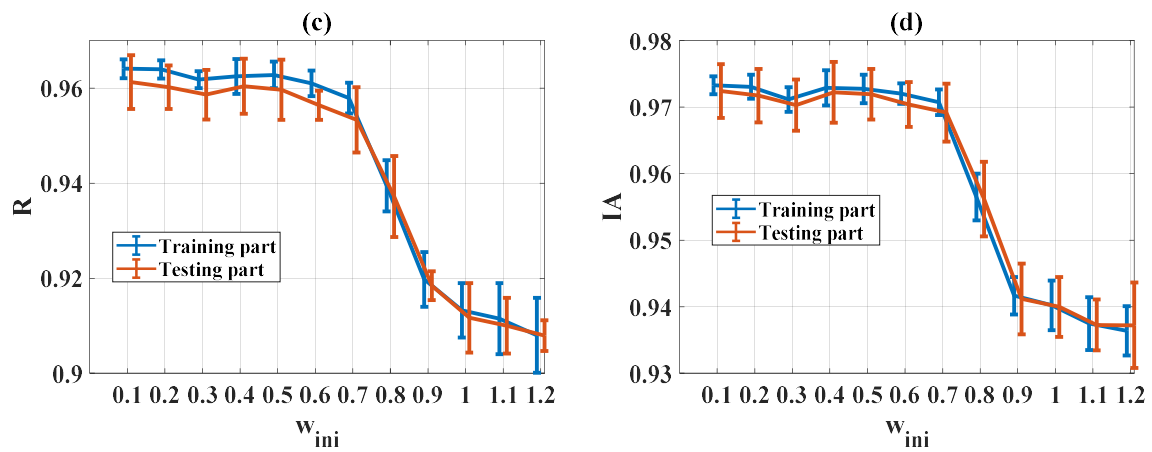


Figure 10. Evaluation of statistical criteria in the function of w_{ini} : (a) RMSE, (b) MAE, (c) R, and (d) IA.

5.3.4. Influence of Personal Learning Coefficient (c_1)

The evaluation of statistical criteria in the function of c_1 for RMSE, MAE, R, and IA is shown in Figure 11a–d, respectively, for both training and testing parts. It can be seen that good prediction performance was obtained when c_1 was in the range of [1, 1.4] for all statistical criteria (RMSE, MAE, R, and IA). Therefore, $c_1 = [1, 1.4]$ was the most appropriate value.

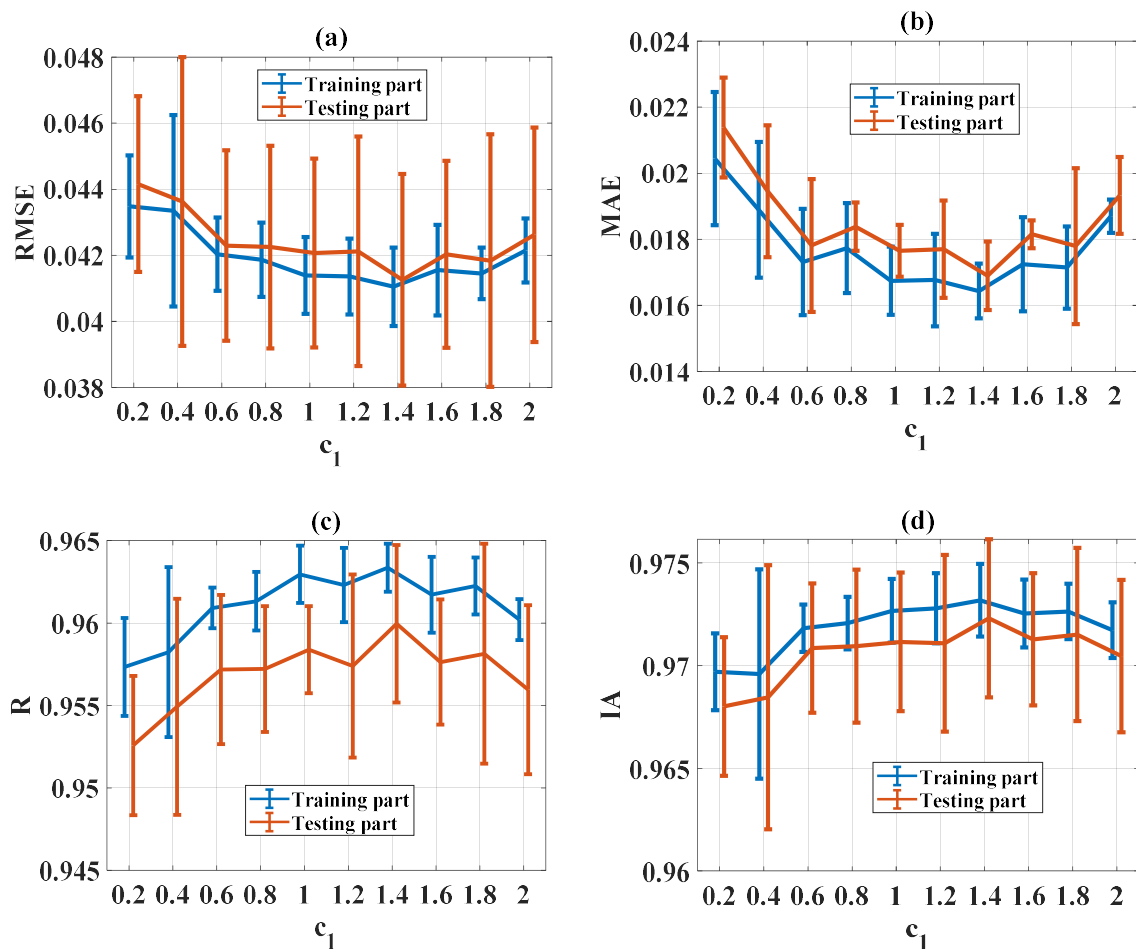


Figure 11. Evaluation of statistical criteria in the function of c_1 : (a) RMSE, (b) MAE, (c) R, and (d) IA.

5.3.5. Influence of Global Learning Coefficient

The evaluation of statistical criteria in the function of c_2 for RMSE, MAE, R, and IA is shown in Figure 12a–d, respectively, for both training and testing parts. It can be seen that good prediction performance was obtained when c_2 was higher than 1.8 for all statistical criteria (RMSE, MAE, R, and IA). Therefore, $c_2 = [1.8, 2]$ was the most appropriate value.

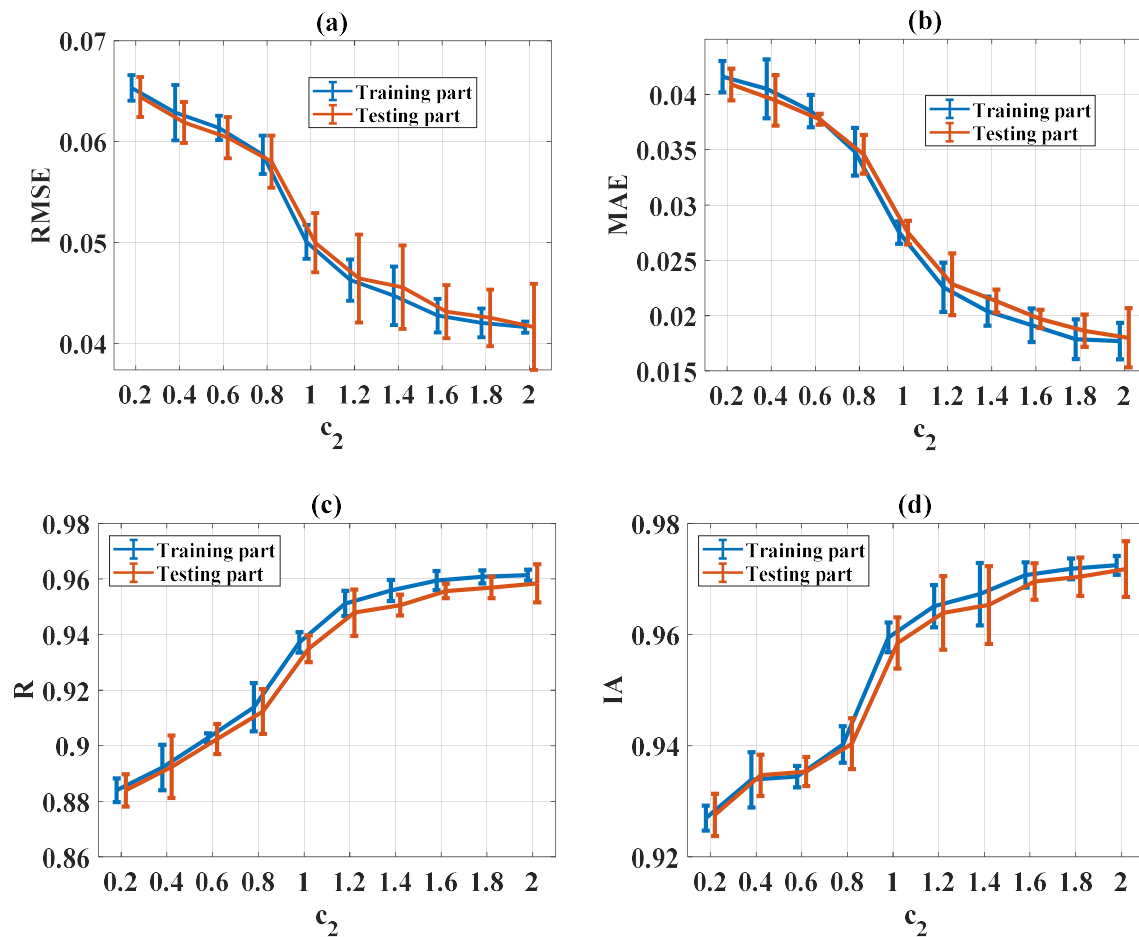


Figure 12. Evaluation of statistical criteria in the function of c_2 : (a) RMSE, (b) MAE, (c) R, and (d) IA.

5.3.6. Influence of Velocity Limits

The evaluation of statistical criteria in the function of f_v for RMSE, MAE, R, and IA is shown in Figure 13a–d, respectively, for both training and testing parts. It can be seen that no influence could be established regarding all statistical criteria (RMSE, MAE, R, and IA). Therefore, $f_v = 0.1$ was finally chosen.

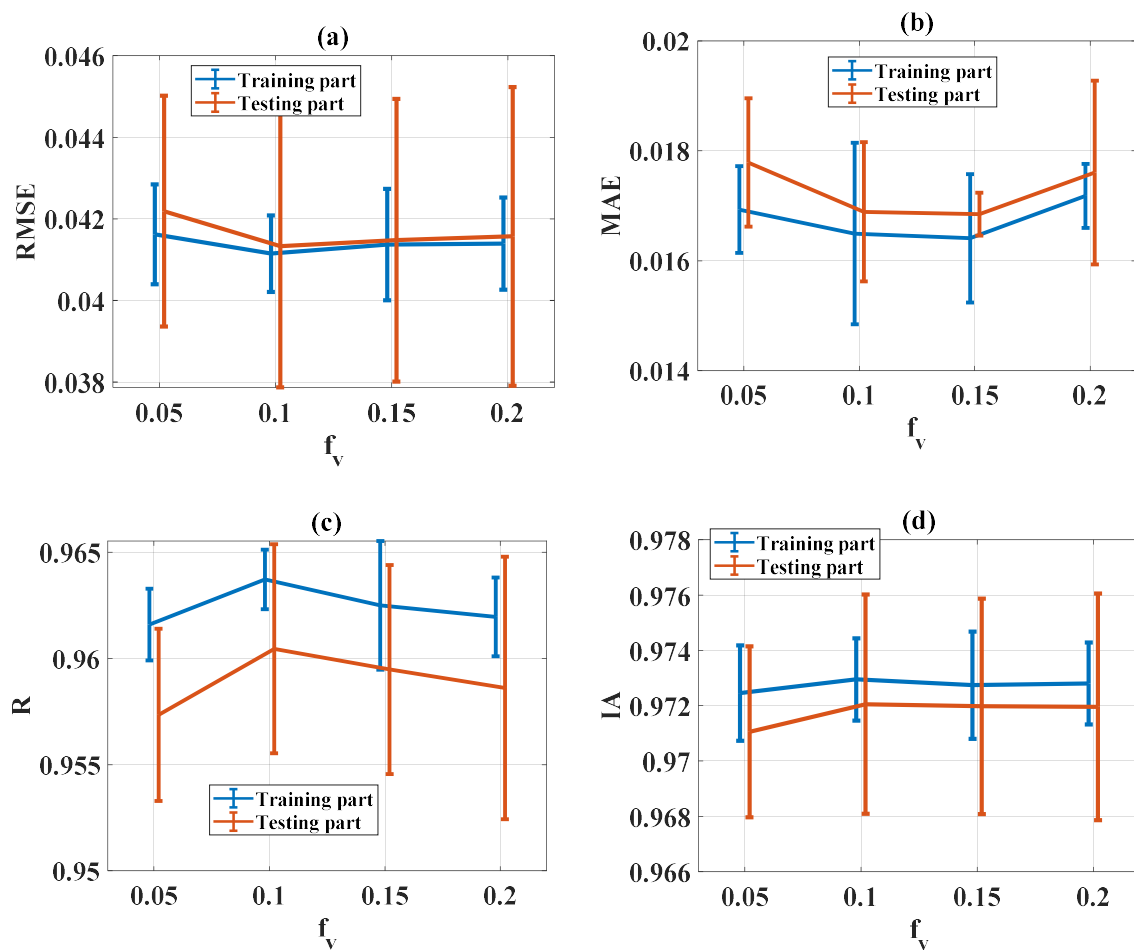


Figure 13. Evaluation of statistical criteria in the function of f_v : (a) RMSE, (b) MAE, (c) R and (d) IA.

5.4. Prediction Capability of the ANFIS-PSO Model using Optimal Configuration

Table 4 summarizes all of the optimal values, as identified previously. By using the optimal coefficient in Table 4, a regression graph between the real and predicted P_u (kN) is shown in Figure 14. The slope of the ideal fit was then used to measure the angle between the x -axis and the ideal fit, with angles closer than 45° showing better performance. Figure 14a shows the predictability when using the training set, whereas Figure 14b shows the same information applied to the testing set. In both cases, the angles generated by the predicted output had slopes close to that of the ideal fit. This showed that the performance of the proposed model was consistent. Figure 15 shows the error distribution graph using the training part, testing part, and all data. In short, using the selected number of fuzzy rules and PSO parameters, the prediction model gave excellent results (Table 5).

Table 4. Parameters used as optimum.

Parameter	Optimal Value	Final Selection
n_{rule}	10	10
n_{pop}	50	50
w_{ini}	0.1–0.4	0.4
c_1	1–1.4	1
c_2	1.8–2	2
f_v	0.1	0.1

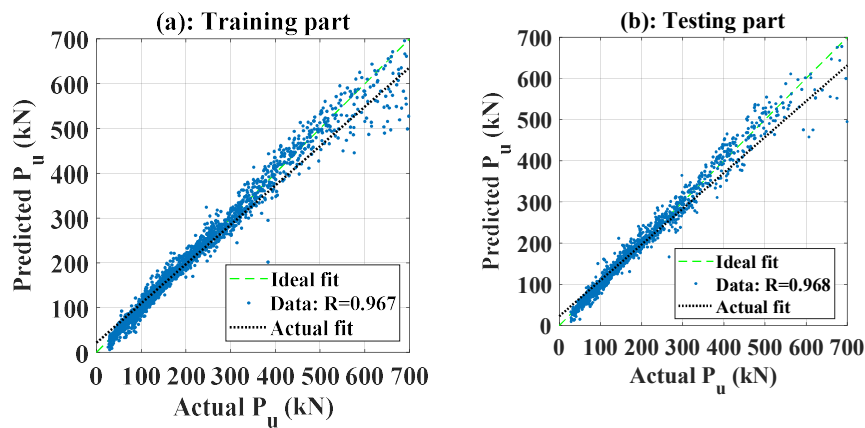


Figure 14. Graphs of regression plots between actual and predicted P_u (kN) for the (a) training part and (b) testing part.

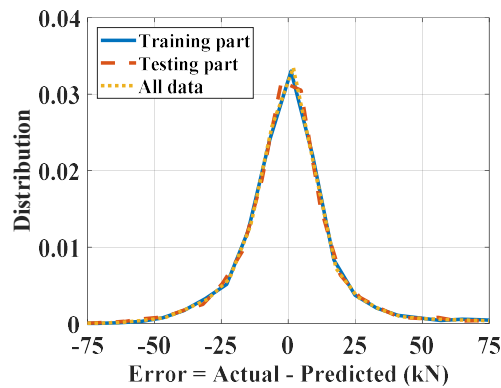


Figure 15. Distribution of errors.

Table 5. Prediction capability.

Part	RMSE	MAE	R	IA	Error Mean	Error Std	Running Time
Training	0.040	0.015	0.967	0.976	0.006	0.039	8 min
Testing	0.037	0.014	0.968	0.977	0.005	0.037	

5.5. Sensitivity Analysis

The sensitivity analysis was performed in order to explore the degree of importance of each input variable using the ANFIS-PSO model. For this, quantile values at 21 points (from 0% to 100%, with a step of 5%) of each input variable were collected from the database and served as a new dataset for the calculation of critical buckling load. More precisely, for a given input, its value varied from 0% to 100%, while all other inputs remained at their median (50%). This variation of values following the probability distribution allows the influence of each input variable to be explored based on their statistical behavior. The results of the sensitivity analysis are indicated in Figure 16 in a bar graph (scaled into the range of 0% to 100%). It can be seen that all variables influenced the prediction of critical buckling load through the ANFIS-PSO model. The most important input variables were L , w_{flange} , t_{web} , and t_{flange} , which gave degree of importance values of 33.9%, 21.7%, 18.6%, and 10.6%, respectively. This information is strongly relevant and in good agreement with the literature, in which the length of the beam and geometrical parameter of the cross-section are the most important parameters [3–5]. However, it can be seen in Figure 16 that the height of the beam does not seriously affect the buckling capacity of the structural members. It should be noted that only three independent values of the section’s height were used to generate the database; for example, 420, 560, and 700 mm. Consequently, the linear correlation coefficient between the section’s height and the buckling capacity was only -0.092 .

On the contrary, the minimum value of the beam's length was 4000 mm (approximately 5.7 times larger than the maximum section's height) and five independent values were used to generate the database, ranging from 4000 to 8000 mm, with a step of 1000 mm. Thus, the linear correlation coefficient between the beam's length and the buckling capacity was -0.667 (approximately 7.25 times bigger than the linear correlation coefficient between the section's height and the buckling capacity). Consequently, a larger database should be considered in future studies to estimate the degree of importance of the section's height.

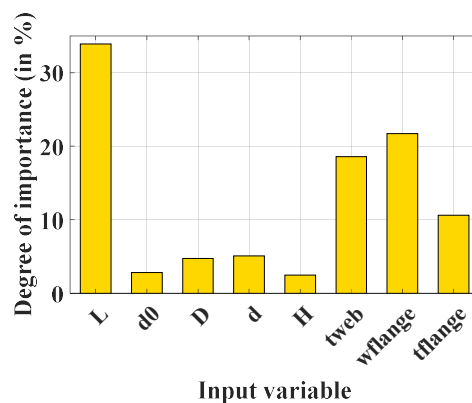


Figure 16. Bar graph showing the estimations of degree of importance values.

The sensitivity analysis presented above demonstrates that the ML technique could assist in the design phase for circular opening steel beams. In addition to reliable prediction of the critical buckling load, the ANFIS-PSO model can also assist in the creation of input–output maps, as illustrated in Figure 17. In particular, as L , t_{web} , w_{flange} , and t_{flange} were the most important variables, they are used for map illustrations in this section. The values of the remaining variables were kept constant. In Figure 17, four maps of critical buckling load are presented (with the same color range), involving the relationship between P_u and L - w_{flange} , L - t_{flange} , L - t_{web} , and w_{flange} - t_{flange} , respectively. As can be seen from the surface plots, the input–output relationship exhibited nonlinear behavior, which cannot be easily identified from the database. Figure 17a shows that a maximum value for the critical buckling load can be obtained if L reaches its minimum and w_{flange} reaches its maximum value. On the other hand, the critical buckling load reaches its minimum if L reaches its highest value and w_{flange} reaches its lowest value. This map confirms the negative effect of L , as pointed out in the literature [4]. In Figure 17b,c, the same results are obtained as in Figure 17a. This observation again confirms that the geometrical parameters of the cross-section are highly important [1,5]. Such quantitative information allows the design and analysis recommendations to be explored, as well as for new beam configurations to be generated (within the range of variables considered in this present study).

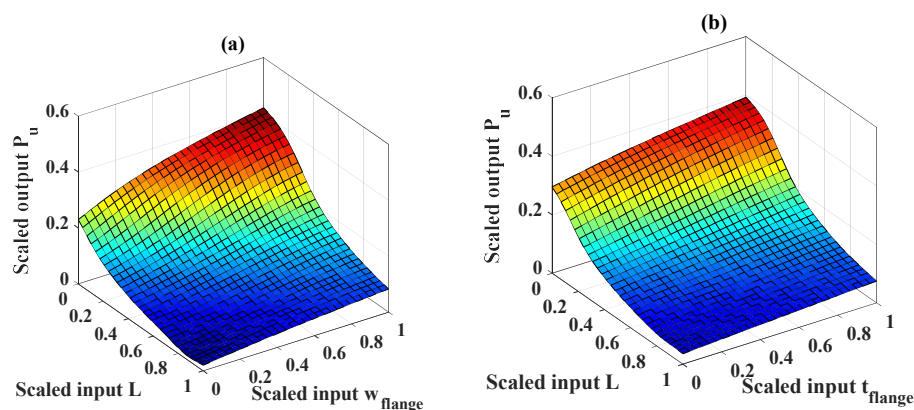


Figure 17. Cont.

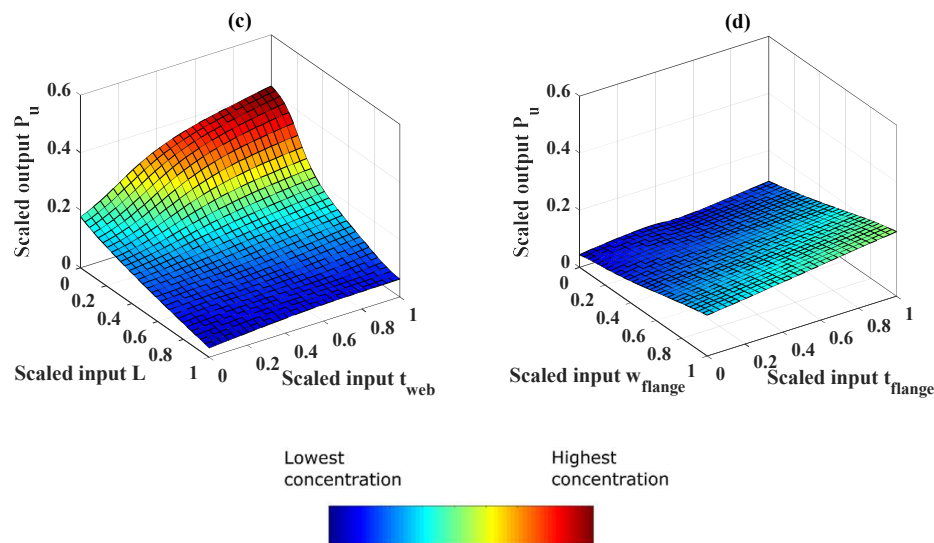


Figure 17. Three-dimensional scaled input–output maps: (a) L - w_{flange} , (b) L - t_{flange} , (c) L - t_{web} , and (d) w_{flange} - t_{flange} .

6. Conclusions

PSO is one of the most popular optimization techniques used to optimize and improve the performance of machine learning models in terms of classification and regression. However, its effectiveness depends significantly on the selection of parameters used to train this technique. In this paper, investigation and selection of PSO parameters was carried out to improve and optimize the performance of the ANFIS model, which is one of the most popular and effective ML models, for prediction of the buckling capacity of circular opening steel beams. Different parameters (n_{rule} , n_{pop} , w_{ini} , c_1 , c_2 , and f_v) of PSO were tuned on 3645 available data samples to determine the best values for optimization of the performance of ANFIS.

The results show that the performance of ANFIS optimized by PSO (ANFIS-PSO) is suitable for determining the buckling capacity of circular opening steel beams, but is very sensitive under different PSO investigation and selection parameters. The results also show that $n_{rule} = 10$, $n_{pop} = 50$, $w_{ini} = 0.1$ to 0.4 , $c_1 = [1, 1.4]$, $c_2 = [1.8, 2]$, and $f_v = 0.1$ are the most suitable selection settings in order to get the best performance from ANFIS-PSO. The sensitivity analysis shows that L , w_{flange} , t_{web} , and t_{flange} are the most important input variables used for prediction of the buckling capacity of circular opening steel beams.

In short, this study might help in selection of the suitable PSO parameters for optimization of ANFIS in determining the buckling capacity of circular opening steel beams. It also helps in suitable selection of input variables for better prediction of the buckling capacity of circular opening steel beams. However, it is noted that the optimal values of PSO parameters found in this study are suitable for the ANFIS model in determining the buckling capacity of circular opening steel beams. Thus, it is suggested that these parameters should be validated with other ML models applied in other problems. Finally, variation in the mechanical properties of material used should be investigated in further research, as this is important from a physics perspective.

Author Contributions: Conceptualization, Q.H.N., H.-B.L., T.-T.L., and B.T.P; methodology, H.-B.L., T.-T.L., and B.T.P; validation, H.-B.L. and T.-T.L; formal analysis, Q.H.N., V.Q.T., T.-A.N., V.-H.P., and H.-B.L; data curation, V.Q.T., T.-A.N., and V.-H.P; writing—original draft preparation, all authors; writing—review and editing, H.-B.L., T.-T.L., and B.T.P; visualization, H.-B.L., T.-A.N., V.-H.P. and T.-T.L; supervision, Q.H.N., H.-B.L., T.-T.L., and B.T.P; project administration, H.-B.L., T.-T.L., and B.T.P; funding acquisition, Q.H.N. All authors have read and agreed to the published version of the manuscript.

Funding: This research received no external funding

Conflicts of Interest: The authors declare no conflict of interest.

Abbreviations

Symbol	Explanation	SI Unit
ANFIS	Adaptive neuro-fuzzy inference system	
PSO	Particle swarm optimization	
R	Correlation coefficient	
RMSE	Root mean squared error	
MAE	Mean absolute error	
IA	Index of agreement	
CV	Coefficient of variation	%
n_{rule}	Number of fuzzy rules	
n_{pop}	PSO population size	
w_{ini}	PSO initial weight	
c_1	PSO cognition learning rate	
c_2	PSO social learning rate	
f_v	PSO velocity limits	

References

- Grilo, L.F.; Fakury, R.H.; de Souza Veríssimo, G. Design procedure for the web-post buckling of steel cellular beams. *J. Constr. Steel Res.* **2018**, *148*, 525–541. [[CrossRef](#)]
- Hoffman, R.; Dinehart, D.; Gross, S.; Yost, J. Analysis of stress distribution and failure behavior of cellular beams. In Proceedings of the International Ansys Conference, Pittsburgh, PA, USA, 2–4 May 2006.
- Sonck, D.; Belis, J. Lateral–torsional buckling resistance of cellular beams. *J. Constr. Steel Res.* **2015**, *105*, 119–128. [[CrossRef](#)]
- Panedpojaman, P.; Thepchatri, T. Finite element investigation on deflection of cellular beams with various configurations. *Int. J. Steel Struct.* **2013**, *13*, 487–494. [[CrossRef](#)]
- Sweedan, A.M. Elastic lateral stability of I-shaped cellular steel beams. *J. Constr. Steel Res.* **2011**, *67*, 151–163. [[CrossRef](#)]
- Ellobody, E. Nonlinear analysis of cellular steel beams under combined buckling modes. *Thin-Walled Struct.* **2012**, *52*, 66–79. [[CrossRef](#)]
- Abidin, A.Z.; Izzuddin, B.A. Meshless local buckling analysis of steel beams with irregular web openings. *Eng. Struct.* **2013**, *50*, 197–206. [[CrossRef](#)]
- Gandomi, A.H.; Tabatabaei, S.M.; Moradian, M.H.; Radfar, A.; Alavi, A.H. A new prediction model for the load capacity of castellated steel beams. *J. Constr. Steel Res.* **2011**, *67*, 1096–1105. [[CrossRef](#)]
- Tsavdaridis, K.D.; D’Mello, C. Web buckling study of the behaviour and strength of perforated steel beams with different novel web opening shapes. *J. Constr. Steel Res.* **2011**, *67*, 1605–1620. [[CrossRef](#)]
- Redwood, R.; Cho, S.H. Design of steel and composite beams with web openings. *J. Constr. Steel Res.* **1993**, *25*, 23–41. [[CrossRef](#)]
- Chung, K.F.; Liu, T.C.H.; Ko, A.C.H. Investigation on Vierendeel mechanism in steel beams with circular web openings. *J. Constr. Steel Res.* **2001**, *57*, 467–490. [[CrossRef](#)]
- Chung, K.F.; Liu, C.H.; Ko, A.C.H. Steel beams with large web openings of various shapes and sizes: An empirical design method using a generalised moment-shear interaction curve. *J. Constr. Steel Res.* **2003**, *59*, 1177–1200. [[CrossRef](#)]
- Nseir, J.; Lo, M.; Sonck, D.; Somja, H.; Vassart, O.; Boissonnade, N. Lateral torsional buckling of cellular steel beams. In Proceedings of the Annual Stability Conference Structural Stability Research Council, Grapevine, TX, USA, 18–21 April 2012; pp. 18–21.
- Ghasemain, B.; Asl, D.T.; Pham, B.T.; Avand, M.; Nguyen, H.D.; Janizadeh, S. Shallow landslide susceptibility mapping: A comparison between classification and regression tree and reduced error pruning tree algorithms. *Vietnam J. Earth Sci.* **2020**. [[CrossRef](#)]
- Ly, H.-B.; Pham, B.T. Prediction of Shear Strength of Soil Using Direct Shear Test and Support Vector Machine Model. *Open Constr. Build. Technol. J.* **2020**, *14*.

16. Pham, B.T.; Phong, T.V.; Nguyen-Thoi, T.; Parial, K.; K. Singh, S.; Ly, H.-B.; Nguyen, K.T.; Ho, L.S.; Le, H.V.; Prakash, I. Ensemble modeling of landslide susceptibility using random subspace learner and different decision tree classifiers. *Geocarto Int.* **2020**, 1–23. [[CrossRef](#)]
17. Nguyen, P.T.; Ha, D.H.; Avand, M.; Jaafari, A.; Nguyen, H.D.; Al-Ansari, N.; Phong, T.V.; Sharma, R.; Kumar, R.; Le, H.V. Soft Computing Ensemble Models Based on Logistic Regression for Groundwater Potential Mapping. *Appl. Sci.* **2020**, *10*, 2469. [[CrossRef](#)]
18. Ly, H.-B.; Le, T.-T.; Vu, H.-L.T.; Tran, V.Q.; Le, L.M.; Pham, B.T. Computational Hybrid Machine Learning Based Prediction of Shear Capacity for Steel Fiber Reinforced Concrete Beams. *Sustainability* **2020**, *12*, 2709. [[CrossRef](#)]
19. Nguyen, P.T.; Ha, D.H.; Nguyen, H.D.; Van Phong, T.; Trinh, P.T.; Al-Ansari, N.; Le, H.V.; Pham, B.T.; Ho, L.S.; Prakash, I. Improvement of Credal Decision Trees Using Ensemble Frameworks for Groundwater Potential Modeling. *Sustainability* **2020**, *12*, 2622. [[CrossRef](#)]
20. Pham, B.T.; Bui, D.T.; Prakash, I.; Nguyen, L.H.; Dholakia, M. A comparative study of sequential minimal optimization-based support vector machines, vote feature intervals, and logistic regression in landslide susceptibility assessment using GIS. *Environ. Earth Sci.* **2017**, *76*, 371. [[CrossRef](#)]
21. Pham, B.T.; Tien Bui, D.; Pham, H.V.; Le, H.Q.; Prakash, I.; Dholakia, M.B. Landslide Hazard Assessment Using Random SubSpace Fuzzy Rules Based Classifier Ensemble and Probability Analysis of Rainfall Data: A Case Study at Mu Cang Chai District, Yen Bai Province (Viet Nam). *J Indian Soc. Remote Sens.* **2017**, *45*, 673–683. [[CrossRef](#)]
22. Feng, S.; Zhou, H.; Dong, H. Using deep neural network with small dataset to predict material defects. *Mater. Des.* **2019**, *162*, 300–310. [[CrossRef](#)]
23. Guo, S.; Yu, J.; Liu, X.; Wang, C.; Jiang, Q. A predicting model for properties of steel using the industrial big data based on machine learning. *Comput. Mater. Sci.* **2019**, *160*, 95–104. [[CrossRef](#)]
24. Nguyen, H.-L.; Le, T.-H.; Pham, C.-T.; Le, T.-T.; Ho, L.S.; Le, V.M.; Pham, B.T.; Ly, H.-B. Development of Hybrid Artificial Intelligence Approaches and a Support Vector Machine Algorithm for Predicting the Marshall Parameters of Stone Matrix Asphalt. *Appl. Sci.* **2019**, *9*, 3172. [[CrossRef](#)]
25. Dao, D.V.; Jaafari, A.; Bayat, M.; Mafi-Gholami, D.; Qi, C.; Moayedi, H.; Phong, T.V.; Ly, H.-B.; Le, T.-T.; Trinh, P.T.; et al. A spatially explicit deep learning neural network model for the prediction of landslide susceptibility. *Catena* **2020**, *188*, 104451. [[CrossRef](#)]
26. Qi, C.; Ly, H.-B.; Chen, Q.; Le, T.-T.; Le, V.M.; Pham, B.T. Flocculation-dewatering prediction of fine mineral tailings using a hybrid machine learning approach. *Chemosphere* **2020**, *244*, 125450. [[CrossRef](#)]
27. Dou, J.; Yunus, A.P.; Merghadi, A.; Shirzadi, A.; Nguyen, H.; Hussain, Y.; Avtar, R.; Chen, Y.; Pham, B.T.; Yamagishi, H. Different sampling strategies for predicting landslide susceptibilities are deemed less consequential with deep learning. *Sci. Total Environ.* **2020**, *720*, 137320. [[CrossRef](#)]
28. Qi, C.; Zhou, W.; Lu, X.; Luo, H.; Pham, B.T.; Yaseen, Z.M. Particulate matter concentration from open-cut coal mines: A hybrid machine learning estimation. *Environ. Pollut.* **2020**, *263*, 114517. [[CrossRef](#)]
29. Tian, J.; Qi, C.; Sun, Y.; Yaseen, Z.M.; Pham, B.T. Permeability prediction of porous media using a combination of computational fluid dynamics and hybrid machine learning methods. *Eng. Comput.* **2020**, 1–17. [[CrossRef](#)]
30. Nguyen, H.Q.; Ly, H.-B.; Tran, V.Q.; Nguyen, T.-A.; Le, T.-T.; Pham, B.T. Optimization of Artificial Intelligence System by Evolutionary Algorithm for Prediction of Axial Capacity of Rectangular Concrete Filled Steel Tubes under Compression. *Materials* **2020**, *13*, 1205. [[CrossRef](#)]
31. Ly, H.-B.; Le, L.M.; Duong, H.T.; Nguyen, T.C.; Pham, T.A.; Le, T.-T.; Le, V.M.; Nguyen-Ngoc, L.; Pham, B.T. Hybrid Artificial Intelligence Approaches for Predicting Critical Buckling Load of Structural Members under Compression Considering the Influence of Initial Geometric Imperfections. *Appl. Sci.* **2019**, *9*, 2258. [[CrossRef](#)]
32. Ly, H.-B.; Le, T.-T.; Le, L.M.; Tran, V.Q.; Le, V.M.; Vu, H.-L.T.; Nguyen, Q.H.; Pham, B.T. Development of Hybrid Machine Learning Models for Predicting the Critical Buckling Load of I-Shaped Cellular Beams. *Appl. Sci.* **2019**, *9*, 5458. [[CrossRef](#)]
33. KhalilzadeVahidi, E.; Rahimi, F. Investigation of Ultimate Shear Capacity of RC Deep Beams with Opening using Artificial Neural Networks. *Adv. Comput. Sci. Int. J.* **2016**, *5*, 57–65.
34. Abambres, M.; Rajana, K.; Tsavdaridis, K.; Ribeiro, T. Neural Network-based formula for the buckling load prediction of I-section cellular steel beams. *Computers* **2019**, *8*, 2. [[CrossRef](#)]

35. Blachowski, B.; Pnevmatikos, N. Neural Network Based Vibration Control of Seismically Excited Civil Structures. *Period. Polytech. Civ. Eng.* **2018**, *62*, 620–628. [[CrossRef](#)]
36. Pnevmatikos, N.G.; Thomos, G.C. Stochastic structural control under earthquake excitations. *Struct. Control Health Monit.* **2014**, *21*, 620–633. [[CrossRef](#)]
37. Seitllari, A.; Naser, M.Z. Leveraging artificial intelligence to assess explosive spalling in fire-exposed RC columns. *Comput. Concr.* **2019**, *24*, 271–282. [[CrossRef](#)]
38. Naser, M.Z. Deriving temperature-dependent material models for structural steel through artificial intelligence. *Constr. Build. Mater.* **2018**, *191*, 56–68. [[CrossRef](#)]
39. Basarir, H.; Elchalakani, M.; Karrech, A. The prediction of ultimate pure bending moment of concrete-filled steel tubes by adaptive neuro-fuzzy inference system (ANFIS). *Neural Comput. Appl.* **2019**, *31*, 1239–1252. [[CrossRef](#)]
40. Naderpour, H.; Mirrashid, M. Shear Strength Prediction of RC Beams Using Adaptive Neuro-Fuzzy Inference System. *Sci. Iran.* **2018**, *27*, 657–670. [[CrossRef](#)]
41. Güneyisi, E.M. A study on estimation of flexural overstrength factor for thin-walled CHS beams using ANFIS. In Proceedings of the 12th International Congress on Advances in Civil Engineering (ACE 2016), Istanbul, Turkey, 21–23 September 2016; Volume 8, pp. 1–7.
42. Oliveira, A.L.; Braga, P.L.; Lima, R.M.; Cornélio, M.L. GA-based method for feature selection and parameters optimization for machine learning regression applied to software effort estimation. *Inf. Softw. Technol.* **2010**, *52*, 1155–1166. [[CrossRef](#)]
43. Saini, L.M. Peak load forecasting using Bayesian regularization, Resilient and adaptive backpropagation learning based artificial neural networks. *Electr. Power Syst. Res.* **2008**, *78*, 1302–1310. [[CrossRef](#)]
44. Rahman, M.A.; Hoque, M.A. Online self-tuning ANN-based speed control of a PM DC motor. *IEEE/ASME Trans. Mechatron.* **1997**, *2*, 169–178. [[CrossRef](#)]
45. Liu, Y.; Yao, X. A population-based learning algorithm which learns both architectures and weights of neural networks. *Chin. J. Adv. Softw. Res.* **1996**, *3*, 54–65.
46. Salem, F.; Awadallah, M.A. Parameters estimation of photovoltaic modules: Comparison of ANN and ANFIS. *Int. J. Ind. Electron. Drives* **2014**, *1*, 121–129. [[CrossRef](#)]
47. Wei, M.; Bai, B.; Sung, A.H.; Liu, Q.; Wang, J.; Cather, M.E. Predicting injection profiles using ANFIS. *Inf. Sci.* **2007**, *177*, 4445–4461. [[CrossRef](#)]
48. Chen, W.; Panahi, M.; Pourghasemi, H.R. Performance evaluation of GIS-based new ensemble data mining techniques of adaptive neuro-fuzzy inference system (ANFIS) with genetic algorithm (GA), differential evolution (DE), and particle swarm optimization (PSO) for landslide spatial modelling. *Catena* **2017**, *157*, 310–324. [[CrossRef](#)]
49. Chen, M.-Y. A hybrid ANFIS model for business failure prediction utilizing particle swarm optimization and subtractive clustering. *Inf. Sci.* **2013**, *220*, 180–195. [[CrossRef](#)]
50. Kiranyaz, S.; Ince, T.; Gabbouj, M. *Multidimensional Particle Swarm Optimization for Machine Learning and Pattern Recognition*; Springer: Berlin/Heidelberg, Germany, 2014; ISBN 3-642-37846-3.
51. Ahmadi, M.A.; Soleimani, R.; Lee, M.; Kashiwao, T.; Bahadori, A. Determination of oil well production performance using artificial neural network (ANN) linked to the particle swarm optimization (PSO) tool. *Petroleum* **2015**, *1*, 118–132. [[CrossRef](#)]
52. Bagheri, A.; Peyhani, H.M.; Akbari, M. Financial forecasting using ANFIS networks with quantum-behaved particle swarm optimization. *Expert Syst. Appl.* **2014**, *41*, 6235–6250. [[CrossRef](#)]
53. Melgani, F.; Bazi, Y. Classification of electrocardiogram signals with support vector machines and particle swarm optimization. *IEEE Trans. Inf. Technol. Biomed.* **2008**, *12*, 667–677. [[CrossRef](#)] [[PubMed](#)]
54. Rini, D.P.; Shamsuddin, S.M.; Yuhaziz, S.S. Particle swarm optimization for ANFIS interpretability and accuracy. *Soft Comput.* **2016**, *20*, 251–262. [[CrossRef](#)]
55. Jang, J.-S. ANFIS: Adaptive-network-based fuzzy inference system. *IEEE Trans. Syst. Man Cybern.* **1993**, *23*, 665–685. [[CrossRef](#)]
56. Haykin, S.; Network, N. A comprehensive foundation. *Neural Netw.* **2004**, *2*, 41.
57. Bui, D.T.; Tsangaratos, P.; Ngo, P.-T.T.; Pham, T.D.; Pham, B.T. Flash flood susceptibility modeling using an optimized fuzzy rule based feature selection technique and tree based ensemble methods. *Sci. Total Environ.* **2019**, *668*, 1038–1054. [[CrossRef](#)] [[PubMed](#)]

58. Kisi, O. Suspended sediment estimation using neuro-fuzzy and neural network approaches/Estimation des matières en suspension par des approches neurofloues et à base de réseau de neurones. *Hydrol. Sci. J.* **2005**, *50*. [[CrossRef](#)]
59. Nguyen, H.-L.; Pham, B.T.; Son, L.H.; Thang, N.T.; Ly, H.-B.; Le, T.-T.; Ho, L.S.; Le, T.-H.; Tien Bui, D. Adaptive Network Based Fuzzy Inference System with Meta-Heuristic Optimizations for International Roughness Index Prediction. *Appl. Sci.* **2019**, *9*, 4715. [[CrossRef](#)]
60. Dao, D.V.; Ly, H.-B.; Trinh, S.H.; Le, T.-T.; Pham, B.T. Artificial Intelligence Approaches for Prediction of Compressive Strength of Geopolymer Concrete. *Materials* **2019**, *12*, 983. [[CrossRef](#)]
61. Mansouri, I.; Ozbakkaloglu, T.; Kisi, O.; Xie, T. Predicting behavior of FRP-confined concrete using neuro fuzzy, neural network, multivariate adaptive regression splines and M5 model tree techniques. *Mater. Struct.* **2016**, *49*, 4319–4334. [[CrossRef](#)]
62. Eberhart, R.; Kennedy, J. A new optimizer using particle swarm theory. In Proceedings of the MHS'95, Proceedings of the Sixth International Symposium on Micro Machine and Human Science, Nagoya, Japan, 4–6 October 1995; pp. 39–43.
63. Termeh, S.V.R.; Khosravi, K.; Sartaj, M.; Keesstra, S.D.; Tsai, F.T.-C.; Dijkema, R.; Pham, B.T. Optimization of an adaptive neuro-fuzzy inference system for groundwater potential mapping. *Hydrogeol. J.* **2019**, *27*, 2511–2534. [[CrossRef](#)]
64. Jaafari, A.; Panahi, M.; Pham, B.T.; Shahabi, H.; Bui, D.T.; Rezaie, F.; Lee, S. Meta optimization of an adaptive neuro-fuzzy inference system with grey wolf optimizer and biogeography-based optimization algorithms for spatial prediction of landslide susceptibility. *Catena* **2019**, *175*, 430–445. [[CrossRef](#)]
65. Zhou, J.; Nekouie, A.; Arslan, C.A.; Pham, B.T.; Hasanipanah, M. Novel approach for forecasting the blast-induced AOp using a hybrid fuzzy system and firefly algorithm. *Eng. Comput.* **2019**. [[CrossRef](#)]
66. Yildiz, A.R. A new hybrid particle swarm optimization approach for structural design optimization in the automotive industry. *Proc. Inst. Mech. Eng. Part D J. Automob. Eng.* **2012**, *226*, 1340–1351. [[CrossRef](#)]
67. He, Q.; Wang, L. An effective co-evolutionary particle swarm optimization for constrained engineering design problems. *Eng. Appl. Artif. Intell.* **2007**, *20*, 89–99. [[CrossRef](#)]
68. Pathak, N.N.; Mahanti, G.K.; Singh, S.K.; Mishra, J.K.; Chakraborty, A. Synthesis of thinned planar circular array antennas using modified particle swarm optimization. *Prog. Electromagn. Res.* **2009**, *12*, 87–97. [[CrossRef](#)]
69. Guillemot, J.; Le, T.T.; Soize, C. Stochastic framework for modeling the linear apparent behavior of complex materials: Application to random porous materials with interphases. *Acta Mech. Sin.* **2013**, *29*, 773–782. [[CrossRef](#)]
70. Pham, B.T.; Nguyen, M.D.; Dao, D.V.; Prakash, I.; Ly, H.-B.; Le, T.-T.; Ho, L.S.; Nguyen, K.T.; Ngo, T.Q.; Hoang, V.; et al. Development of artificial intelligence models for the prediction of Compression Coefficient of soil: An application of Monte Carlo sensitivity analysis. *Sci. Total Environ.* **2019**, *679*, 172–184. [[CrossRef](#)]
71. Le, T.T.; Guillemot, J.; Soize, C. Stochastic continuum modeling of random interphases from atomistic simulations. Application to a polymer nanocomposite. *Comput. Methods Appl. Mech. Eng.* **2016**, *303*, 430–449. [[CrossRef](#)]
72. Pham, B.T.; Nguyen-Thoi, T.; Ly, H.-B.; Nguyen, M.D.; Al-Ansari, N.; Tran, V.-Q.; Le, T.-T. Extreme Learning Machine Based Prediction of Soil Shear Strength: A Sensitivity Analysis Using Monte Carlo Simulations and Feature Backward Elimination. *Sustainability* **2020**, *12*, 2339. [[CrossRef](#)]
73. Hun, D.-A.; Guillemot, J.; Yvonnet, J.; Bornert, M. Stochastic multiscale modeling of crack propagation in random heterogeneous media. *Int. J. Numer. Methods Eng.* **2019**, *119*, 1325–1344. [[CrossRef](#)]
74. Capillon, R.; Desceliers, C.; Soize, C. Uncertainty quantification in computational linear structural dynamics for viscoelastic composite structures. *Comput. Methods Appl. Mech. Eng.* **2016**, *305*, 154–172. [[CrossRef](#)]
75. Le, M.V.; Yvonnet, J.; Feld, N.; Detrez, F. The Coarse Mesh Condensation Multiscale Method for parallel computation of heterogeneous linear structures without scale separation. *Comput. Methods Appl. Mech. Eng.* **2020**, *363*, 112877. [[CrossRef](#)]
76. Tran, V.P.; Brisard, S.; Guillemot, J.; Sab, K. Mori–Tanaka estimates of the effective elastic properties of stress-gradient composites. *Int. J. Solids Struct.* **2018**, *146*, 55–68. [[CrossRef](#)]
77. Staber, B.; Guillemot, J.; Soize, C.; Michopoulos, J.; Iliopoulos, A. Stochastic modeling and identification of a hyperelastic constitutive model for laminated composites. *Comput. Methods Appl. Mech. Eng.* **2019**, *347*, 425–444. [[CrossRef](#)]

78. Tran, V.-P.; Guilleminot, J.; Brisard, S.; Sab, K. Stochastic modeling of mesoscopic elasticity random field. *Mech. Mater.* **2016**, *93*, 1–12. [[CrossRef](#)]
79. Soize, C.; Desceliers, C.; Guilleminot, J.; Le, T.-T.; Nguyen, M.-T.; Perrin, G.; Allain, J.-M.; Gharbi, H.; Duhamel, D.; Funfschilling, C. Stochastic representations and statistical inverse identification for uncertainty quantification in computational mechanics. In Proceedings of the UNCECOMP 2015—1st ECCOMAS Thematic Conference on Uncertainty Quantification in Computational Sciences and Engineering, Crete Island, Greece, 25–27 May 2015; pp. 1–26.
80. Le, T.-T.; Guilleminot, J.; Soize, C. Stochastic continuum modeling of random interphases from atomistic simulations. In Proceedings of the Euromech 559, Multi-Scale Computational Methods for Bridging Scales in Materials and Structures, Eindhoven, The Netherlands, 23–25 February 2015; pp. 1–2.
81. Christian, P.d.S. (Ed.) *Stochastic Models of Uncertainties in Computational Mechanics*; American Society of Civil Engineers: Reston, VA, USA, 2012; ISBN 978-0-7844-1223-7.
82. Dao, D.V.; Ly, H.-B.; Vu, H.-L.T.; Le, T.-T.; Pham, B.T. Investigation and Optimization of the C-ANN Structure in Predicting the Compressive Strength of Foamed Concrete. *Materials* **2020**, *13*, 1072. [[CrossRef](#)] [[PubMed](#)]
83. Le, T.-T. Modélisation Stochastique, en Mécanique des Milieux Continus, de l'Interphase Inclusion-Matrice à Partir de Simulations en Dynamique Moléculaire. Ph.D. Thesis, University of Paris-Est Marne-la-Vallée, Paris, France, 2015.
84. Le, T.-T.; Pham, B.T.; Le, V.M.; Ly, H.-B.; Le, L.M. A Robustness Analysis of Different Nonlinear Autoregressive Networks Using Monte Carlo Simulations for Predicting High Fluctuation Rainfall. In *Proceedings of the Micro-Electronics and Telecommunication Engineering*; Sharma, D.K., Balas, V.E., Son, L.H., Sharma, R., Cengiz, K., Eds.; Springer: Singapore, 2020; pp. 205–212.
85. Dao, D.V.; Adeli, H.; Ly, H.-B.; Le, L.M.; Le, V.M.; Le, T.-T.; Pham, B.T. A Sensitivity and Robustness Analysis of GPR and ANN for High-Performance Concrete Compressive Strength Prediction Using a Monte Carlo Simulation. *Sustainability* **2020**, *12*, 830. [[CrossRef](#)]
86. Pham, B.T.; Jaafari, A.; Prakash, I.; Bui, D.T. A novel hybrid intelligent model of support vector machines and the MultiBoost ensemble for landslide susceptibility modeling. *Bull. Eng. Geol. Environ.* **2019**, *78*, 2865–2886. [[CrossRef](#)]
87. Ly, H.-B.; Desceliers, C.; Le, L.M.; Le, T.-T.; Pham, B.T.; Nguyen-Ngoc, L.; Doan, V.T.; Le, M. Quantification of Uncertainties on the Critical Buckling Load of Columns under Axial Compression with Uncertain Random Materials. *Materials* **2019**, *12*, 1828. [[CrossRef](#)]
88. Le, L.M.; Ly, H.-B.; Pham, B.T.; Le, V.M.; Pham, T.A.; Nguyen, D.-H.; Tran, X.-T.; Le, T.-T. Hybrid Artificial Intelligence Approaches for Predicting Buckling Damage of Steel Columns Under Axial Compression. *Materials* **2019**, *12*, 1670. [[CrossRef](#)]
89. Pham, B.T.; Le, L.M.; Le, T.-T.; Bui, K.-T.T.; Le, V.M.; Ly, H.-B.; Prakash, I. Development of advanced artificial intelligence models for daily rainfall prediction. *Atmos. Res.* **2020**, *237*, 104845. [[CrossRef](#)]
90. Le, V.M.; Pham, B.T.; Le, T.-T.; Ly, H.-B.; Le, L.M. Daily Rainfall Prediction Using Nonlinear Autoregressive Neural Network. In *Proceedings of the Micro-Electronics and Telecommunication Engineering*; Sharma, D.K., Balas, V.E., Son, L.H., Sharma, R., Cengiz, K., Eds.; Springer: Singapore, 2020; pp. 213–221.
91. Pham, B.T.; Nguyen, M.D.; Ly, H.-B.; Pham, T.A.; Hoang, V.; Van Le, H.; Le, T.-T.; Nguyen, H.Q.; Bui, G.L. Development of Artificial Neural Networks for Prediction of Compression Coefficient of Soft Soil. In *Proceedings of the CIGOS 2019, Innovation for Sustainable Infrastructure*; Ha-Minh, C., Dao, D.V., Benboudjema, F., Derrible, S., Huynh, D.V.K., Tang, A.M., Eds.; Springer: Singapore, 2020; pp. 1167–1172.
92. Tran, V.Q.; Nguyen, H.L.; Dao, V.D.; Hilloulin, B.; Nguyen, L.K.; Nguyen, Q.H.; Le, T.-T.; Ly, H.-B. Temperature effects on chloride binding capacity of cementitious materials. *Mag. Concr. Res.* **2019**, 1–39. [[CrossRef](#)]
93. Pham, B.T.; Singh, S.K.; Ly, H.-B. Using Artificial Neural Network (ANN) for prediction of soil coefficient of consolidation. *Vietnam J. Earth Sci.* **2020**. [[CrossRef](#)]
94. Ly, H.-B.; Asteris, P.G.; Pham, B.T. Accuracy assessment of extreme learning machine in predicting soil compression coefficient. *Vietnam J. Earth Sci.* **2020**. [[CrossRef](#)]
95. Ly, H.-B.; Monteiro, E.; Le, T.-T.; Le, V.M.; Dal, M.; Regnier, G.; Pham, B.T. Prediction and Sensitivity Analysis of Bubble Dissolution Time in 3D Selective Laser Sintering Using Ensemble Decision Trees. *Materials* **2019**, *12*, 1544. [[CrossRef](#)] [[PubMed](#)]

96. Montavon, G.; Rupp, M.; Gobre, V.; Vazquez-Mayagoitia, A.; Hansen, K.; Tkatchenko, A.; Müller, K.-R.; Lilienfeld, O.A. von Machine learning of molecular electronic properties in chemical compound space. *New J. Phys.* **2013**, *15*, 095003. [[CrossRef](#)]
97. Ly, H.-B.; Le, L.M.; Phi, L.V.; Phan, V.-H.; Tran, V.Q.; Pham, B.T.; Le, T.-T.; Derrible, S. Development of an AI Model to Measure Traffic Air Pollution from Multisensor and Weather Data. *Sensors* **2019**, *19*, 4941. [[CrossRef](#)]
98. Ly, H.-B.; Pham, B.T.; Dao, D.V.; Le, V.M.; Le, L.M.; Le, T.-T. Improvement of ANFIS Model for Prediction of Compressive Strength of Manufactured Sand Concrete. *Appl. Sci.* **2019**, *9*, 3841. [[CrossRef](#)]
99. Le, T.-T.; Pham, B.T.; Ly, H.-B.; Shirzadi, A.; Le, L.M. Development of 48-hour Precipitation Forecasting Model using Nonlinear Autoregressive Neural Network. In *Proceedings of the CIGOS 2019, Innovation for Sustainable Infrastructure*; Ha-Minh, C., Dao, D.V., Benboudjema, F., Derrible, S., Huynh, D.V.K., Tang, A.M., Eds.; Springer: Singapore, 2020; pp. 1191–1196.
100. Qi, C.; Tang, X.; Dong, X.; Chen, Q.; Fourie, A.; Liu, E. Towards Intelligent Mining for Backfill: A genetic programming-based method for strength forecasting of cemented paste backfill. *Miner. Eng.* **2019**, *133*, 69–79. [[CrossRef](#)]
101. Kim, S.; Kim, H. A new metric of absolute percentage error for intermittent demand forecasts. *Int. J. Forecast.* **2016**, *32*, 669–679. [[CrossRef](#)]
102. He, X.; Guan, H.; Qin, J. A hybrid wavelet neural network model with mutual information and particle swarm optimization for forecasting monthly rainfall. *J. Hydrol.* **2015**, *527*, 88–100. [[CrossRef](#)]



© 2020 by the authors. Licensee MDPI, Basel, Switzerland. This article is an open access article distributed under the terms and conditions of the Creative Commons Attribution (CC BY) license (<http://creativecommons.org/licenses/by/4.0/>).